i_NRACM: Incorporating ^{15}N into the Regional Atmospheric Chemistry Mechanism (RACM) for assessing the role photochemistry plays in controlling the isotopic composition of NO_x, NO_y, and atmospheric nitrate.

Greg Michalski. *Purdue University, Department of Earth, Atmospheric, and Planetary Sciences, Department of Chemistry. West Lafayette, IN. USA*

Huan Fang. *Purdue University, Department of Earth, Atmospheric, and Planetary Sciences. West Lafayette, IN. USA*

Wendell Walters. *Brown University, Institute for Environment and Society*

David Mase. *Purdue University, Department of Earth, Atmospheric, and Planetary Sciences. West Lafayette, IN. USA*

Key Points

- Modeling nitrogen isotope fractionation during the photochemical oxidation of nitrogen oxides into atmospheric nitrate.

- Incorporation of N isotopes of NOy into the Regional Atmospheric Chemistry Mechanism.

- Implications for quantifying NO_x sources and oxidation pathways using nitrogen isotopes.

Abstract

Nitrogen oxides, classified as NO_x (nitric oxide (NO) + nitrogen dioxide (NO_2)) and NO_y (NO_x + NO_3, N_2O_5 HNO_3, + HNO_4 + HONO + Peroxyacetyl nitrate (PAN) + organic nitrates + any oxidized N compound), are important trace gases in the troposphere, which play an important role in the formation of ozone, particulate matter (PM), and secondary organic aerosols (SOA). Among many uncertainties in movement of atmospheric N compounds, nowadays understanding of NO_y cycling is limited by NO_x emission budget, unresolved issues within the heterogeneous uptake coefficients of N_2O_5, the formation of organic nitrates in urban forests, etc. A photochemical mechanism used to simulate tropospheric photochemistry was altered to include ^{15}N compounds and reactions as a means to simulate δ^{15}N values in NO_y compounds. The 16 N compounds and 96 reactions involving N used in Regional Atmospheric Chemistry Mechanism (RACM) were replicated using ^{15}N in a new mechanism called i_NRACM. The 192 N reactions in i_NRACM were tested to see if isotope effects were relevant with respect to significantly changing the δ^{15}N values (+/- 1‰) of NO_x, HONO, and/or HNO_3. The isotope fractionation factors (α) for relevant reactions were assigned based on recent experimental or calculated values. Each relevant reaction in the i_NRACM mechanism was tested individually and in concert in order to assess the controlling reactions. The final mechanism was characterized by running simulations under different conditions that are typical of pristine, rural, urban, and highly polluted environments. The results of these simulations predicted several interesting δ^{15}N variations.

1. Introduction

Nitrogen oxides are an integral part of atmospheric chemistry, controlling the oxidation state of the troposphere, influencing aerosol formation, altering the pH of rainwater, and facilitating the movement of nitrogen through the N cycle. Nitrogen oxides are classified as NO_x (nitric oxide (NO) + nitrogen dioxide (NO_2)) and NO_y ($NO_x + NO_3$, N_2O_5 HNO_3, + HNO_4 + HONO + Peroxyacetyl nitrate (PAN) + organic nitrates + any oxidized N compound) [*Day et al.*, 2003; *Harrison et al.*, 1999; *Hegglin et al.*, 2006; *Ma et al.*, 2013]. NO_x produces ozone (O_3) through NO_2 photolysis, and NO acts as a catalyst in O_3 production when volatile organic compounds (VOCs) are present. In turn, O_3 photolysis generates OH radicals, which initiates a radical chain reaction involving HO_2 and organic peroxide propagators that result in the oxidation of chemically reduced compounds in the troposphere making them more soluble [*Finlayson-Pitts and Pitts*, 2000; *Seinfeld and Pandis*, 1998]. Thus, NO_x facilitates the cleansing of the atmosphere through the production of O_3 and OH_x (OH + HO_2), which together define the troposphere's oxidation state [*Bloss et al.*, 2005; *Lelieveld et al.*, 2008; *Prinn*, 2003]. These oxidants play an important role in the formation of particulate matter (PM) [*Bauer et al.*, 2007; *Pye et al.*, 2010], forming secondary organic aerosols (SOA) via VOC oxidation [*Hoyle et al.*, 2011; *Shrivastava et al.*, 2017]. They also generate secondary inorganic PM through NO_x, sulfur oxides (SO_x), and ammonia (NH_3) neutralization, which leads to ammonium nitrate (NH_4NO_3) and ammonium sulfate (($NH_4)_2SO_4$) production [*Cao et al.*, 2017; *Pan et al.*, 2018; *Pusede et al.*, 2016]. The production of PM has important consequences for air quality aerosols [*Andreae and Crutzen*, 1997], human health [*Bruningfann and Kaneene*, 1993; *Hall et al.*, 1992], and radiative forcing [*Charlson et al.*, 1992; *Chen et al.*, 2007]. Termination reactions in NO_y cycling produces HNO_3, and facilitates the production of sulfuric acid (H_2SO_4), two strong acids that decrease the pH of rain, known colloquially as acid rain and impact aerosol pH, both of which triggers a number of negative impacts on the environment [*Brimblecombe et al.*, 2007; *Lajtha and Jones*, 2013]. When NO_y is deposited to the surface by wet and dry deposition, it transfers bioavailable N to ecosystems that may be bereft of, or saturated with, bioavailable N. This process can shift the balance of both terrestrial and aquatic ecosystems and impact the goods and services that those ecosystems can normally deliver [*Du et al.*, 2019; *E. M. Elliott et al.*, 2019; *Fowler et al.*, 2013]. Thus, understanding NO_y sources and their chemistry is important for an array of scientific disciplines and evaluating their social, economic, and cultural impact on the environment.

Despite this importance, there are numerous knowledge gaps in the understanding of the cycling of NO_y in the atmosphere. The NO_x emission budget is still poorly constrained. Most emission inventories rely on fixed emission factors for some sources that may, in fact, be variable. For example, power plant NO_x emissions are based on assumed efficiency of catalytic converters that may not be accurate [*Srivastava et al., 2005; Felix et al., 2012*]. Soil NO emissions are highly dependent on soils moisture, redox conditions, fertilizer application rates, type, and timing making them challenging to constrain [*Shepherd, 1991; Galloway et al., 2004; Hudman et al., 2012; Houlton et al., 2013; Pilegaard, 2013*]. There are several unresolved issues with the heterogeneous uptake coefficients of N_2O_5 [*Brown et al.*, 2001; *Brown et al.*, 2006; *Chang et al.*, 2011] and the formation of organic nitrates in urban forests [*Lee et al., 2016; Romer et al., 2016; Kastler and Ballschmiter*, 1998]. The relative importance and mechanism of HONO formation versus HONO emissions are also hotly debated. Likewise, reactions of NO_y in the aqueous phase and mixed aerosols are not fully understood. Chemical transport models (CTMs) do not accurately predict

aerosol nitrate concentrations or other NO_y mixing ratios [*Spak and Holloway*, 2009; *Zhang et al.*, 2009]. Therefore, it is important that these uncertainties in NO_y cycling be resolved if we aim to have accurate air quality forecast and accurate chemistry-climate models that use CTMs.

It has been suggested that stable N isotopes can provide clues as to the origin of NO_x [*Elliott et al.*, 2009; *Felix and Elliott*, 2014; *Walters et al.*, 2015b] and the oxidation pathways that transform in NO_y [*Walters and Michalski*, 2015; 2016]. Isotopic measurements of NO_y compounds show a wide range of $\delta^{15}N$ values (Eq. (1)), which has been suggested to indicate variability in NO_x emission sources, chemical processing, and/or a combination of these effects. $\delta^{15}N$ is defined by the relative difference between the $^{15}N/^{14}N$ ratio in a NO_y compound and the ratio in air N_2 (the arbitrary reference compound) and is typically reported in parts per thousand e.g. per mil (‰)

$$\delta^{15}N_{NOy} (‰) = [(^{15}NO_y/^{14}NO_y) / (^{15}N_2/^{14}N_2) -1]*1000 \qquad \text{Eq. (1)}$$

A number of studies have measured the $\delta^{15}N$ values of NO_x collected from NO_x sources such as power plants [*Felix et al.*, 2012], automobiles [*Walters et al.*, 2015a], biomass burning [*Fibiger and Hastings*, 2016], and non-road sources [*Felix and Elliott*, 2014].

Many studies have measured the $\delta^{15}N$ values of various NO_y compounds collected from the troposphere. Most of the NO_y $\delta^{15}N$ data is for nitrate that has been collected on filters (PM$_{2.5}$, PM$_{10}$, TSP) [*Moore, 1977; Savard et al., 2017*], as the dissolved NO_3^- anion in rain [*Heaton, 1987; Hastings et al., 2003; Felix et al., 2015; Yu & Elliott, 2017*], or as gas phase HNO_3 [*Elliott et al., 2009; Savard et al., 2017*]. The range of tropospheric NO_y $\delta^{15}N$ values span -50 to +15‰ but the average is ~0‰. Two hypotheses have been offered to explain these ranges: Source and Photochemistry. The source hypothesis [*Elliott et al., 2007; Hastings et al., 2013*] suggesting that the tropospheric NO_y $\delta^{15}N$ value range reflects the spatial and temporal mixing of NO_x sources with different $\delta^{15}N$ values that is then converted into NO_y. The photochemistry hypothesis [*Freyer*, 1991; *Freyer et al.*, 1993; *Walters et al.*, 2018] suggests that the observed NO_y $\delta^{15}N$ variations arise via isotope effects occurring when photochemical cycling partitions N into the myriad of NO_y compounds. These two hypotheses are not mutually exclusive. Indeed it is likely to be a combination of both processes, but their relative importance likely shifts depending on environmental conditions such as a region's NO_x source diversity, plume versus dispersed chemistry, photolysis intensity, and oxidant load. In turn, the $\delta^{15}N$ data might be a new key to reconciling some of the current uncertainties in NO_y sources and chemistry, if it can be properly interpreted.

What has become clear is that the temporal-spatial heterogeneity of NO_x sources and the complex photochemistry of NO_y presents a serious challenge to deciphering the observed NO_y $\delta^{15}N$ values. Except for a few isolated cases, a proper assessment of NO_y $\delta^{15}N$ values will require incorporating isotope effects into 3-D chemical transport models. This will include emission modeling of $^{15}NO_x$, meteorological mixing, factoring in isotope effects during NO_y removal processes, and developing chemical mechanisms that incorporate ^{15}N compounds and their relative rate constants. Here we take the first step in this endeavor by developing a chemical mechanism (0-D photochemical box model) that explicitly includes $^{15}NO_y$ compounds and the isotope effects that occur during their cycling through photolysis, equilibrium, and kinetic reactions.

2. Methods

2.1 Chemical and isotopic compounds and reactions included in i_NRACM

The basis of the i_NRACM model is incorporating ^{15}N into the Regional Atmospheric Chemistry Mechanism (RACM) detailed in Stockwell et al. [*Stockwell et al.*, 1997]. RACM is an extension of the chemical mechanism used in the Regional Acid Deposition Model (RADM2) [*Stockwell et al.*, 1990], but with updated inorganic and organic chemistry. There are 17 stable inorganic compounds, 4 inorganic intermediates, 32 stable organic compounds, including 4 biogenic organics, and 24 organic intermediates in the RACM mechanism. The RACM mechanism uses 237 chemical reactions, including 23 photolysis reactions [*Atkinson, 1990; Atkinson et al., 1992*]. The rate constants, photolysis cross-sections and quantum yields for the inorganic compounds were taken from [*DeMore et al.*, 1994]. The RACM mechanism aggregates the thousands of VOC in the atmosphere into 16 anthropogenic and 3 biogenic organic compounds. Part of the aggregation criteria is based on the reactivity of a VOC towards the hydroxyl radical (•OH). Full details on how •OH reacts with alkanes, alkenes, aromatics, and other VOCs, and the aggregation rationale, can be found in Stockwell et al. (*1997*). The actinic flux model used in RACM was developed by Madronich (*1987*) and calculates the wavelength-dependent photon flux as a function of solar zenith angle, which is a function of time (hourly), date, latitude, and longitude. Inputs to the model include temperature, water vapor content, pressure, initial gas mixing ratios and primary pollutant emission rates. Complete details on the RACM mechanism can be found in Stockwell et al. (*1997*).

Our i_NRACM (isotope N in RACM) mechanism was generated by adding ^{15}N isotopologues for the 2 primary (NO, NO_2) and the 14 secondary N pollutants found in the original RACM mechanism (Table S1a). By definition, an isotopologue is a compound with the same chemical formula but a different mass (e.g. NO = 30 amu and ^{15}NO = 31 amu, with N = ^{14}N). This is different from isotopomers, which are isotopic isomers, compounds with the same mass but a different structure caused by isotopic substitution (e.g. $^{15}NNO_5$ = 109 amu and $N^{15}NO_5$ = 109 amu). Of all the reactive N compounds only N_2O_5 has multiple possible ^{15}N substitutions and 2 isotopologues were defined in the i_NRACM: $^{15}NNO_5$ and $^{15}N^{15}NO_5$. The ^{15}N compounds are numbered (Table S1a) and subscripted (a, b) in order to maintain a compound numbering scheme that is consistent with that in Stockwell et al. (*1997*). The non-N compounds found in both RACM and i_NRACM mechanisms have been excluded from Table S1a for the sake of brevity but can be found in Stockwell et al. (*1997*). The 16 ^{15}N compounds (Table S1a) were added to the original RACM FORTRAN code provided by Stockwell by using Z =^{15}N (e.g. ^{15}NO is defined as ZO).

The 96 chemical reactions involving N compounds (Table S2a-f) were inspected and replicated for ^{15}N based on classification as the reaction being either "N only" or "multiple N" reactions. Single N reactions are those where only one N compound was found in the products and reactants, for example NO + O_3 → NO_2+O_2. Multiple N reactions could have multiple N compounds in the reactants, the products, or both. Examples of these possible multiple N reactions are NO_2+NO_3 → N_2O_5, N_2O_5 → NO_2 + NO_3, and NO_3 + NO → NO_2 + NO_2 respectively. For these multiple N reactions, a reaction probability was factored into the isotopologue/isotopomer rate constants (discussed below). For example, the N isotopologue/isotopomer equivalent of the N_2O_5 →NO_2 + NO_3 reaction has two isotopomer reactions: $^{15}NNO_5$ →$^{15}NO_2$ + NO_3 and $^{15}NNO_5$→NO_2 + $^{15}NO_3$. These two isotopologue rate constants (R54a, R54b) are multiplied by a factor of 1/2 to account for this statistical probability. Similar statistical factors were considered when N compounds or intermediates decomposed or reacted to form multiple N products (R52a, R52b, R52c, R52d). All N isotopologue reaction stoichiometry is given in Table S2a-f.

2.2 Isotope effects included in i_NRACM

4

The main challenge for developing realistic isotopologue chemistry in i_NRACM is quantifying the differences in rate constants caused by isotopic substitution. These isotope effects can be classified into four general types: Equilibrium isotope effects (EIE), kinetic isotope effects (KIE), photo-induced isotope fractionation effects (PHIFE), and vapor pressure isotope effects (VPIE). For this study, the most up-to-date isotope fractionations were used when establishing the framework for modeling their effect associated with NO_x oxidation chemistry. The established framework will easily enable an adjustment of isotope effects as we improve our understanding of isotope fractionation factors.

Urey *(1947)* and Bigelesien and Mayer *(1947)* showed that EIEs are driven by the sensitivity of molecular and condensed-phase vibrational frequencies to isotopic substitutions [*Bigeleisen and Mayer*, *1947; Urey, 1947*]. Because vibrations are used in the molecular partition function (Q) to calculate equilibrium constants, isotopic substitution results in isotopologues having different equilibrium constants. Urey [*1947*] defined the reduced partition function ratio for two isotopologues of the same compound as a β value. For example, the reduced partition function ratio of nitric oxide N isotopologues is $Q_{15NO}/Q_{NO} = \beta_{NO}$, with the heavy isotope placed in the numerator by convention. The ratio of two β values is denoted as $\alpha_{\beta1/\beta2}$ the isotope fractionation factor. For example, $\alpha_{NO/NO2}$ is the temperature-dependent isotope fractionation factor (EIE) for the NO + $^{15}NO_2 \longleftrightarrow ^{15}NO + NO_2$. In this case, at 298K $\beta_{NO} = 1.0669$ and $\beta_{NO2} = 1.1064$ and $\alpha_{NO/NO2} = \beta_{NO}/\beta_{NO2} = 0.9643$ [*Walters and Michalski, 2015*].

A KIE is the relative change in the rate of a unidirectional chemical reaction when one of the atoms of the reactants is substituted with an isotope [*Bigeleisen and Wolfsberg*, *1958*]. KIEs are driven by the change in energy required to proceed over the reaction barrier (transition state) as well as changes in the probability of quantum mechanical tunneling [*Wolfsberg et* al., *2010*]. This generally results in a lighter isotopologue reacting faster than a heavier isotopologue. Much of the early research on KIEs were investigations of the KIE in reactions containing hydrogen isotopes and these studies usually defined a KIE = $k_L/k_{H} = \alpha_{L/H}$, where the k's are the rate constants for the light and heavy isotopologues. This is the inverse of the definition of α usually used in research dealing with EIE, VPIE, PHIFE and this inversion can lead to confusion. In this paper, in order to maintain consistency between the α values for EIE, KIE, VPIE, and PHIFE, α will be defined as heavy/light for all four effects.

The α values for EIE and KIE can be determined using a number of approaches. The α values for EIE can be calculated if molecular constants (e.g. harmonic frequencies and anharmonicity constants) of the isotopologue pair are known. Accurate molecular constants are difficult to accurately measure for large molecules and as a result, they primary exist only for diatomic and triatomic isotopologues [*Richet et al.*, *1977*]. The only experimental EIE values for ^{15}N isotopologues of NO_y is for the EIE between NO and NO_2 [*Sharma et al., 1970; Walters et al., 2016*]. To determine the EIE in other NO_y compounds we must rely on quantum chemistry computation methods to estimate the molecular constants and anharmonicity constants. Recent works utilizing these methods have estimated the EIE for most non-organic NO_y compounds [*Walters and Michalski*, *2015*]. For KIE, in addition to molecular constants, the transition state vibrational frequencies are also needed. The only ^{15}N KIE calculation to date for an NO_y compound is for the KIE for the NO + O_3 reaction [*Walters and Michalski*, *2016*].

These EIE and KIE values have been incorporated in i_NRACM in this study Table S2a-c. If there is no isotope effect associated with any of the NO_y reactions, then α is set equal to 1. The ^{15}N isotopologue rate constant for any reaction is then $\alpha^{14}k$ where ^{14}k is the rate constant for any

[14]N reaction in RACM and these are given in Table S2a-f. It is useful to define the magnitude of EIE and KIE in the same per mil (‰) notation used to quantify a $\delta^{15}N$ values by defining an enrichment factor $\varepsilon(‰) = (\alpha-1)1000$. For example, the NO_x isotope exchange equilibrium mentioned above, the $\varepsilon_{NO/NO2} = -35.7‰$. This means that $^{15}NO/NO$ ratio would be 35.7‰ smaller than the $^{15}NO_2/NO_2$ ratio if the isotopes in two gases were statistically distributed (Table S2b).

PHIFE is the relative change in photolysis rates of isotopologues due to the substitution of a heavier isotope [*Yung and Miller, 1997*]. In the atmospheric N cycle, NO_2, NO_3, N_2O_5, and HONO readily undergo photolysis at wavelengths of light that penetrate into the troposphere. The PHIFE can be estimated using a simple zero-point energy shift model (ΔZPE). In this approximation, the absorption spectra of the heavier isotopologue is generated by applying a uniform blue shift (equal to ΔZPE) to the measured spectral absorbance of the light (major) isotopologue [*Blake et al., 2003; Liang et al., 2004; Miller and Yung, 2000*]. This results in isotopic fractionation because the wavelength (λ) dependent photolysis rate constant ($J(\lambda)$) is dependent on the convolution of the absorption cross-section ($\sigma(\lambda)$), actinic flux ($F(\lambda)$), and quantum yield ($\phi(\lambda)$) (Eq. (2)):

$$^{x}J(\lambda) = {}^{x}\sigma(\lambda)F(\lambda)\phi(\lambda) \quad \text{Eq. (2)}$$

The overall photolysis rate constant (^{z}J) can be calculated by integrating σ, F, and ϕ over a range of wavelengths that can cause dissociation (λ_1 and λ_2):

$$^{x}J = \int_{\lambda_1}^{\lambda_2} {}^{x}\sigma(\lambda)F(\lambda)\phi(\lambda)d\lambda \quad \text{Eq. (3)}$$

The N isotopologue fractionation (α) resulting from photolysis (of NO_2 isotopologues) is calculated by (Eq. (4)).

$$\alpha_{47/46} = \frac{^{47}J}{^{46}J} \quad \text{Eq. (4)}$$

It is important to note that there are limitations in the ΔZPE-shift model [*Blake et al., 2003; Liang et al., 2004; Miller and Yung, 2000*]. These include the failure to account for changes in shape and intensity of absorption spectra upon isotopic substitution and the same quantum yield (as a function of wavelength) is assumed for all isotopologues. Despite these limitations, this approach should still give a rough estimate of photolytic fractionation until experimentally determined PHIFE's become available [*Blake et al.*, 2003; *Liang et al.*, 2004; *Miller and Yung*, 2000].

Isotopologues partition differently between phases giving rise to the VPIE. This is most notable in gas-liquid systems [*Van Hook et al.*, 2001], but also can occur in gas-solid equilibrium. Both of these may ultimately be important for understanding $\delta^{15}N$ variability in NO_y compounds. For example, solid-gas VPIE may be relevant for the $HNO_{3(g)} + NH_{3(g)} \longleftrightarrow NH_4NO_{3(s)}$ reaction, whose temperature-dependent equilibrium can shift dramatically diurnally [*Morino et al., 2006*] and seasonally [*Paulot et al., 2016*]. It is likely that this VPIE will result in the particle phase NO_3^- having a different $\delta^{15}N$ value compared to the gas phase HNO_3 [Heaton, 1987]. Additionally, possible VPIE occurring during wet and dry deposition, such as $HNO_{3(g)} \rightarrow HNO_{3(aq)}$ may be relevant for $\delta^{15}N$ variations NO_3^- in precipitation *[Freyer et al., 1993]*. Multiphase reactions are not included in RACM since it is only concerned with gas phase reactions. These effects may be important for accurate $\delta^{15}N$ predictions and should be addressed in more complex models, but this

is a limitation in any "gas phase only" photochemical box model. Similarly, NO_y aqueous phase reactions, such as $2NO_2 + H_2O \rightarrow HNO_3 + HNO_2$, are not included in RACM, which may limit i_NRACM's ability to accurately predict the $\delta^{15}N$ values of dissolved NO_3^- in rainfall samples.

2.3 Sensitivity analysis: Determining the "reaction relevance" of NO_y isotopologues

The objective of the i_NRACM model is to make predictions about the temporal and spatial variation of $\delta^{15}N$ value in various N compounds caused by EIE, KIE, and PHIFE, and compare them to observations. Currently, the $\delta^{15}N$ observations are largely limited to HNO_3, as either particulate or dissolved NO_3^-, but there are a few recent measurements of the $\delta^{15}N$ values of NO_x [*Walters et al., 2018*] and HONO [*Chai and Hastings, 2018*]. The $\delta^{15}N$ values of organic nitrates and PAN may be made in the not so distant future, but there is no published data to date. Thus, a given isotopologue reaction pair in i_NRACM was considered "relevant" if it significantly changed the $\delta^{15}N$ value (± 1‰) of NO_x, HONO, or HNO_3. This relevance was determined by conducting a sensitivity analysis on the PHIFE, KIE, and EIE effects for all N reactions. This was done by arbitrarily setting $\alpha = 0.98$ ($\varepsilon = -20$‰) for one isotopologue reaction and $\alpha = 1.0$ for all others, then running a test case. This test case is a 5-day simulation, beginning at 3 AM on March 1 (2007) and simulates mid-latitude suburban chemistry using the trace gas and meteorology parameters given in Table S3a-b. This simulation was repeated 96 times until every N containing reaction was tested. For example, NO_x, HONO, or HNO_3 $\delta^{15}N$ values are not sensitive to R51 (Fig. 1). The following section discusses which i_NRACM reactions are relevant and the approaches used to determine the appropriate α values for those reactions. <u>These simulations were also used to test whether i_NRACM achieve N isotope mass balance via $\Sigma^{15}N/\Sigma^{14}N$ where the sums are the ending abundances of all N compounds. This resulted in $\delta^{15}N = 0$ for all simulations.</u>

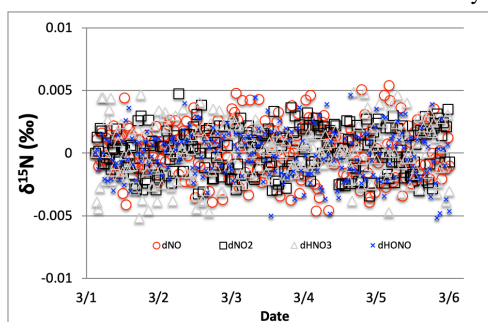Figure 1. The time evolution of $\delta^{15}N$ values of NO, NO_2, HONO, and HNO_3, caused by the $NO_3 + NO \rightarrow NO_2 + NO_2$ reaction (R 51, 51$_a$). This reaction only induces a $\delta^{15}N$ variation of +/- 0.005‰ in the relevant compounds. Thus, this reaction is considered irrelevant and i_NRACM sets R51a $\alpha = 1.0$.

Moved (insertion) [1]

Moved up [1]: These simulations were also used to test whether i_NRACM achieve N isotope mass balance via $\Sigma^{15}N/\Sigma^{14}N$ where the sums are the ending abundances of all N compounds. This resulted in $\delta^{15}N = 0$ for all simulations.

Deleted: ¶
¶

2.3.1 PHIFE relevant in the i_NRACM mechanism

Only one of the 6 photolysis reactions involving N compounds was found to be relevant. NO_2 photolysis (R1) had a significant impact on the $\delta^{15}N$ value of NO_x, HONO, and HNO_3 (Fig. 2). The initial difference between the $\delta^{15}N$ of NO and NO_2 values is roughly equal to the arbitrarily set -20‰ enrichment factor. The nature of the diurnal oscillation in $\delta^{15}N$ values on the three relevant NO_y compounds and the dampening effect over time will be discussed in the results section.

When there is sufficient photolysis of any single NO_y compound, then the $\delta^{15}N$ value of that compound tends to significantly change, but often neither the HNO_3, HONO, nor NO_x $\delta^{15}N$ values are affected. For example, the arbitrary α for NO_3 photolysis (R7 and R8) alters the $\delta^{15}N$ value of HNO_3 and NO_x by less than 0.1‰ (not shown), but it induces a large diurnal changes in the $\delta^{15}N$ value of NO_3 and N_2O_5, with sharp transitions occurring during sunrise and sunset (Fig. 3). This is easily understood. For our test case, during the day $^{15}NO_3$ would be left behind because $^{14}NO_3$ is preferentially being photolyzed. The daytime N_2O_5 formed from this NO_3 (positive $\delta^{15}N$) and NO_2 ($\delta^{15}N \sim 0$) thus has a $\delta^{15}N$ values halfway between these two reactants (isotope mass balance). However, there is so little NO_3 and N_2O_5 during the day that essentially no HNO_3 is being formed through these precursors and the NO_3 PHIFE is not manifested in the NO_x or HNO_3 $\delta^{15}N$ value. During the night, photolysis and the PHIFE ceases and any NO_3 and N_2O_5 formed by NO_2 oxidation have $\delta^{15}N$ values equal to the NO_2.

NO_x, HONO, and HNO_3 are not sensitive to the other NO_y photolysis reactions because of this isotope mass balance effect.

$$\delta^{15}N_{NOy} = \Sigma f_{NOyi} \bullet \delta^{15}N_{NOyi} \quad \text{Eq. (5)}$$

Figure 2. The time evolution of $\delta^{15}N$ values of NO, NO_2, HNO_3, and HONO caused by PHIFE during NO_2 photolysis.

Figure 3. The time evolution of $\delta^{15}N$ values of NO_3, and N_2O_5 caused by PHIFE during NO_3 photolysis.

Where f_{NOyi} is the mole fraction of any NO_{yi} compound relative to total NO_y, $\delta^{15}N_{NOyi}$ is the $\delta^{15}N$ value of that compound, and $\delta^{15}N_{NOy}$ is the value of total N, which in these simulations is arbitrarily set to 0‰. For an $\varepsilon = -20‰$ and a threshold of "importance" set to $\pm$ 1‰, isotope mass balance requires that $f_{NOyi}>0.05$. Only NO, NO_2, HONO, and HNO_3 compounds meet this threshold (Fig. 4). All other f_{NOyi} values are an order of magnitude smaller, the largest being f_{HNO4} and it only reaches a maximum value of 0.005. By the end of the second simulation day the f_{HNO3} has approached 1 and effectively minimizes the other f_{NOyi} values because it is the only stable N compound because the other NO_y compounds are very photochemically active. If we exclude this build up in HNO_3 from the sum of NO_y, then f_{NO}, and f_{NO2} (and HONO during some hours, see discussion) become the dominant fractions (Fig. 4) and they control the other $f_{NOyi.}$ Even under this constraint, the f_{HNO4} only reaches 0.001 (Fig. 4). Thus, in i_NRACM, the α values of α_{R4}- α_{R8}

8

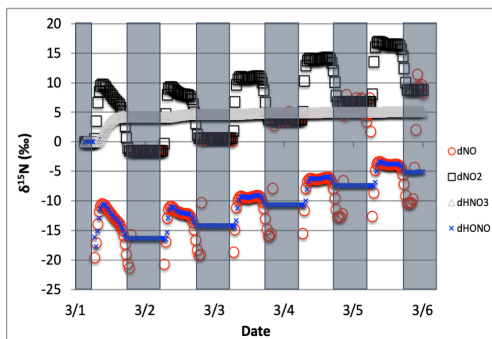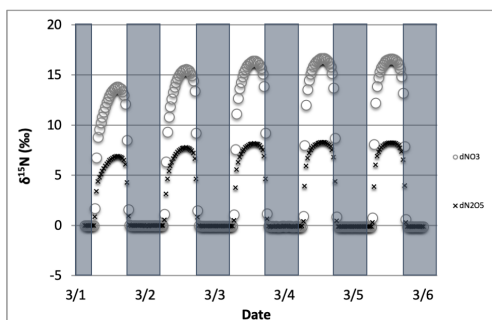were set equal to 1 and only the α_{R1} was assigned a non-1 value, which was determined using a PHIFE theory (discussed below).

2.3.2 KIE relevant in i_NRACM mechanism

The KIE for 12 N containing compounds and their 96 reactions were evaluated using the same sensitivity analysis. The vast majority of reactions had little influence on the $\delta^{15}N$ values of NO_x, HONO, and HNO_3 (Fig. 1). Similar to the photolysis sensitivity, either reaction proximity or isotope mass balance were controlling $\delta^{15}N$ relevance. For example, $NO_2 + OH$ is reaction that directly produces a significant fraction of HNO_3 and therefore R39 is relevant in the i_NRACM mechanism. In contrast, R95 produces very little HNO_3 so it has a negligible influence on the predicted HNO_3 $\delta^{15}N$ value. Therefore, the only relevant KIE reactions that have $\alpha \neq 1$ in i_NRACM mechanism are R39, R91-R97, R48 (Table S2b).

2.3.3 EIE relevant in i_NRACM mechanism

While some EIE are naturally handled in the i_NRACM mechanism, such as the NO_2–NO_3–N_2O_5 equilibrium, other potentially important N isotope exchange reactions are not directly expressed in RACM and must be considered. From a thermodynamic perspective, the EIE for any two N containing compounds can be calculated. The rate at which these compounds can achieve equilibrium, however, needs careful consideration. For example, the EIE for the isotope exchange reaction $NO + {}^{15}HNO_3 \leftrightarrow {}^{15}NO + HNO_3$ has been calculated and measured [*Brown and Begun, 1959*]. Yet, steric considerations would suggest it would be very improbable for a gas phase reaction pathway or transition state to exist where two O atoms and a hydrogen from a HNO_3 could quickly migrate to a NO molecule during a collision. The result is that isotope exchange for this gas phase reaction is likely kinetically too slow to be relevant but is valid in a highly concentrated liquid phase [*Brown and Begun, 1959*]. The larger the N containing molecule the more difficult it is to envision gas phase EIE occurring on a timescale comparable to the residence time tropospheric N of about a week. On the other hand,
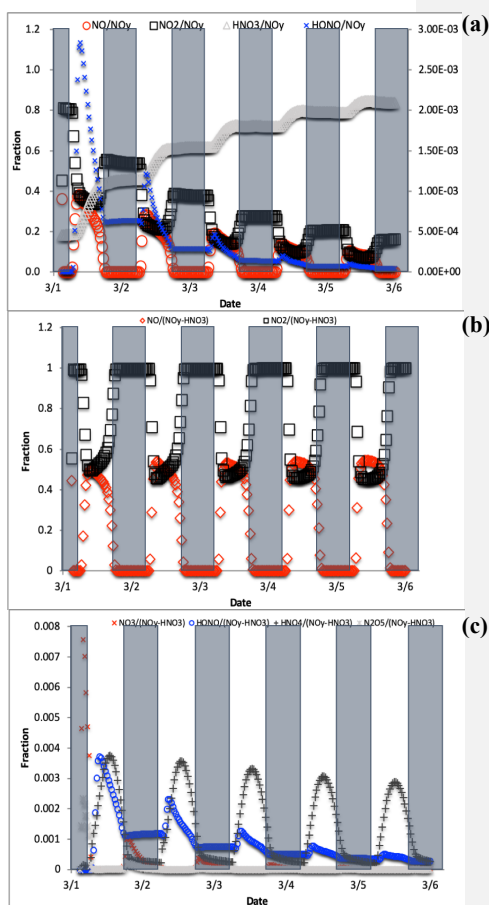
Figure 4. The change in f_{NO}, f_{NO2}, f_{NO3}, and f_{HONO} (right axis) over the 5-day simulation shows the transition from NO_y as mostly NO_x to predominately HNO_3 (top, a). For reactive NO_y (NO_y – HNO_3) large diurnal changes in f_{NO} and f_{NO2} (middle, b) caused by photolysis minimize the other f_{NOy} values, none of which exceeds 0.01 (bottom, c).

the isotope exchange reaction $NO + {}^{15}NO_2 \longleftrightarrow {}^{15}NO + NO_2$ rapidly occurs [*Sharma et al.*, 1970] because it can form an ONONO (N_2O_3) stable intermediate. As such, i_NRACM only considers N isotope equilibrium between NO, NO_2, NO_3, and N_2O_5. Since the latter 3 compounds are already *chemically* equilibrated in RACM, they are by default isotopically equilibrated in i_NRACM. Therefore, the only new isotope exchange reaction added to i_NRACM was $NO + {}^{15}NO_2 \longleftrightarrow {}^{15}NO + NO_2$ (R238, R238a).

2.4 Isotopologue fraction factors (α) used in i_NRACM

In this section we discuss the methodology used to determine the values for the relevant PHIFE, KIE, and EIE. These are reactions R1, R39, R48, R91-R97, and R238.

2.4.1 PHIFE derived α used in the i_NRACM mechanism

The PHIFE for R1 was calculated using existing NO_2 experimental photolysis cross-section of ${}^{14}NO_2$ for tropospheric relevant wavelengths (300 to 450 nm) [*Vandaele* et al., 2002]. Using the experimentally determined ΔZPE for the ${}^{15}NO_2$ isotopologue of 29.79 cm^{-1} [*Michalski et al., 2004*], the ${}^{47}\sigma(\lambda)$ was blue shifted by roughly 0.3 nm from the experimentally measured ${}^{46}\sigma(\lambda)$ [*Vandaele et al., 2002*] (Fig. 5). The wavelength dependent actinic flux, $F(\lambda)$, was taken from the TUV model (NCAR) for solar zenith angles from 0 to 90° in 15° increments. The $\phi(\lambda)$ values were taken from experimental data at 298 K [*Roehl et al.*, 1994], and it was assumed that there is no significant quantum yield isotope effect. Based on these assumptions the ${}^{46}J(\lambda)$ and ${}^{47}J(\lambda)$ values were calculated (Fig. 5). An important feature of NO_2 the wavelength dependent J include a peak near 390-400 nm that subsequently decreases at longer wavelengths until NO_2 photolysis ceases beyond 420 nm due to a $\phi = 0$ beyond this wavelength [*Roehl et al., 1994*]. Overall, the NO_2 PHIFE α value was found to be consistent for the wide range of solar zenith angles, ranging between 1.002 to 1.0042 with higher values occurring at lower solar zenith angles. We used an $\alpha = 1.0042$ for daylight hours.
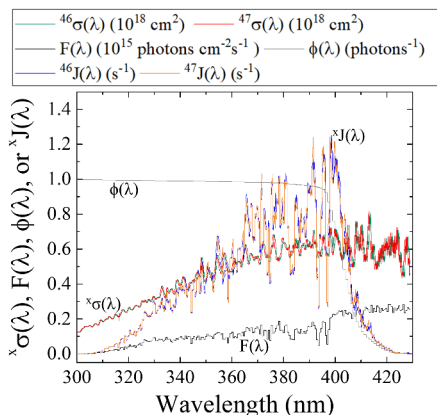

Figure 5. Literature reported ${}^{46}\sigma(\lambda)$ [*Vandaele et al., 2002*] $F(\lambda)$ (at SZA of 60°; TUV model), and NO_2 $\phi(\lambda)$ [*Roehl et al., 1994*] and calculated ${}^{47}\sigma(\lambda)$ derived from the ZPE shift model for wavelengths relevant for tropospheric conditions for NO_2 photolysis. From these parameters, both ${}^{46}J(\lambda)$ and ${}^{47}J(\lambda)$ have been calculated (Eq. 2).

Deleted: (

Deleted:)

2.4.2 KIE derived α used in the i_NRACM mechanism

2.4.2.1 KIE for the $NO + O_3$ reaction

The ${}^{15}\alpha_{48}$ for the reaction $NO + O_3 \rightarrow NO_2 + O_2$ reaction was determined by *ab initio* calculations [*Walters and Michalski*, 2016]. Generally, in a normal KIE the heavy ${}^{15}NO$ would react with O_3 slower than the light ${}^{14}NO$, which consistent with the calculated effect, however, it

is relatively small (ε = -6.7‰ at 298 K). The $^{15}\alpha_{48}$ was determined to have the following temperature dependent relationship [*Walters and Michalski*, 2016] over the temperature range of 220 to 320 K (Eq. (6)):

$$\alpha_{48} = (0.9822*\exp(3.3523/T)) \qquad \text{Eq. (6)}$$

2.4.2.2 KIE for the NO_3 + VOC reactions

The most influential reactions that impacted the $\delta^{15}N$ of HNO_3 were the three reaction pathways that generate HNO_3. This is because the isotope effect associated with this last step is largely retained in the product HNO_3 because photolysis of HNO_3 back into photochemically active compounds that could re-scramble N isotopes is slow, effectively "locking in" these final isotope effects. Two gas phase reactions groups are important for HNO_3 production. Nitric acid is produced mainly by R39 during the daytime [*Seinfeld and Pandis, 1998*] but this reaction is treated as an EIE as discussed below in the EIE section. During the nighttime, when the photolysis sink for NO_3 vanishes, NO_3 can react with VOCs to form HNO_3 via hydrogen abstraction reactions [*Atkinson, 2000*]. Any individual NO_3 + VOC reaction had a small "relevance" for the $\delta^{15}N$ values of NO_x, and HNO_3, but given there are 7 such reactions (R91-R97) their sum may be important.

The KIE for each of the NO_3 +VOC$\rightarrow$ HNO_3 reaction (R91-R97) was determined by assuming collisional frequency was the key KIE factor in such reactions. In these reactions (R91-R97) NO_3 abstracts a hydrogen from a hydrocarbon, acting though a transition state involving the oxygen atoms in the nitrate radical C--H--ONO_2. Since N is not directly participating in the bond formation it is classified as a secondary KIE [*Wolfsberg*, 1960]. Secondary KIE are typically much smaller than primary KIEs that occur at bond breaking/forming positions within a molecule [*Wolfsberg*, 1960]. Therefore, we assumed that the secondary KIE was negligible and did not factor into the α values for these 7 reactions. On the other hand, isotope substitution does change the relative rate of collisions for N isotopologues because of the change in molecular mass. The collisional frequency (Eq.7) for any of the NO_3 + VOC reaction pair was calculated assuming a hard sphere approximation via

$$A = \left[\frac{8kT}{\pi\mu}\right]^{1/2} \pi d^2 \qquad \text{Eq. (7)}$$

here μ is the reduced mass of either NO_3 or $^{15}NO_3$ and the specific hydrocarbon in a given reaction (R91-R97). When taking the isotopologue collision ratio, the constants, collision cross-section (d^2), and temperature cancel out giving a temperature independent KIE of

$$\alpha = \frac{k_{15}}{k_{14}} = \frac{A_{15}}{A_{14}} = \sqrt{\frac{\overline{\mu_{15}}}{\mu_{14}}} \qquad \text{Eq. (8)}$$

The α for each NO_3 + VOC reaction (R91-R97) as calculated using the hydrocarbon mass (Table S1b) and the NO_3 isotopologue masses (62, 63 amu) and using Eq. (8).

2.4.3 EIE derived α used in the i_NRACM mechanism

2.4.3.1 EIE of NO + NO_2 exchange

The NO + NO$_2$ exchange was added to i_NRACM by defining a forward and reverse reaction (R238, R238a) and an equilibrium constant $K_{238} = k_{238}/k_{238a} = \alpha$. The forward rate constant (k_{238}) was based on the NO-NO$_2$ isotope exchange rate determined by Sharma et al. ($3.6*10^{14}$ cm^3 s^{-1} molecule^{-1}). The reverse rate was calculated using $k_{238} = k_{238a}/\alpha_{238}$. The temperature-dependent for EIE of NO + NO$_2$ exchange (Eq. 9) was calculated using quantum mechanical techniques [*Walters and Michalski*, 2015] that matched well with recent experimental values [*Walters et al.*, 2016].

$$\alpha_{238} = 0.9771*\exp(18.467/T) \qquad \text{Eq. (9)}$$

2.4.3.2 EIE used in the NO$_2$ + OH reaction

The $^{15}\alpha_{39}$ for the NO$_2$+OH+M → HNO$_3$ reaction (R39) was determined by assuming equilibrium between NO$_2$ and HNO$_3$. The third body and the negative temperature dependence of the rate constant shows that, similar to O$_3$ formation, this reaction is an association reaction [*Golden and Smith, 2000*]. It proceeds through an excited intermediate, *HNO$_3$, that can undergo collisional deactivation by a third body M (Eq.10).

NO$_2$ + OH $\overset{k_r}{\longleftarrow}$ k_f → *HNO$_3$ k_d→ HNO$_3$ Eq. (10)

in which k_f and k_r are the forward and reverse rate constants for the association step and k_d is the rate constant for collisional quenching and deactivation of the activated complex. We have calculated that k_f/k_d is on the order of 5.5 (see SA) thus the assumption about reactant-complex isotopic equilibrium appears to be valid since only a single decomposition would isotopic equilibrium. The HNO$_3$ production rate constant is then $k_f k_d[M]/k_r = K_{eq}k_d[M]$. This general form can be used to write two isotopologue equilibrium constants K

$K_{39} = [*HNO_3]/([NO_2][OH]) = k_{39f}/k_{39r}$ Eq. (11)
$K_{39a} = [*H^{15}NO_3]/([^{15}NO_2][OH]) = k_{39af}/k_{39ar}$ Eq. (12)

Since •OH is not participating in the N isotope chemistry, these two EIE effectively reduces the isotope chemistry to the temperature dependent ^{15}N EIE
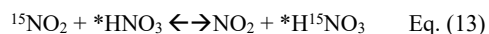
$^{15}NO_2 + *HNO_3 \longleftrightarrow NO_2 + *H^{15}NO_3$ Eq. (13)
$K_{39a}/K_{39} = \alpha_{HNO3/NO2} = \beta_{HNO3}/\beta_{NO2}$ Eq. (14)

The fundamental vibration frequencies for HNO$_3$* were taken to be the same as ground state HNO$_3$, similar to RRKM theory approaches used to calculate the uni-molecular decay rate of HNO$_3$* [*Golden and Smith, 2000*]. The temperature-dependent β_{HNO3} and β_{NO2} values for this exchange were taken from [*Walters and Michalski, 2015*]. Since the reaction has a negative activation energy and has a fairly rapid rate constant at 101 kPa, (1×10^{11} cm^{-3} s^{-1}) and the isotope effect due to the collisional deactivation frequency (Eq. 7) is minimal (~2‰) compared to the equilibrium effect (~40‰), the deactivation rate constants k_d were set equal ($k_{d14}/k_{d15}=1$). Setting $k_{r14}= k_{r15}$, and using the $\alpha_{HNO3/NO2}$ equilibrium value the k_{39a} for the ^{15}NO$_2$ + OH → H^{15}NO$_3$ reaction is

$K_{39a} = \alpha_{HNO3/NO2}(K_{39})$ Eq. (15)

The temperature dependence of $\alpha_{HNO3/NO2}$ is derived from the tables in [*Walters and Michalski*, 2015] and α_{39} is then:

$\alpha_{39} = (0.973*\exp(19.743/T)$ Eq. (16)

For typical tropospheric temperatures the $\alpha_{HNO3/NO2}$ 1.040 suggesting the $\delta^{15}N$ of HNO_3 produced by the $NO_2 + OH$ reaction will be +40‰ relative to tropospheric NO_2. This α value is larger and opposite the sign of the $^{15}\alpha = 0.9971$ assumed by Freyer et al. (*1991*). Freyer's α was Deleted: *3* approximated by the using reduced mass of the OH-NO_2 activated complex. There two problems with this approach. First, the activation complex's reduced mass approximation should be viewed in terms as the *decomposition* rate constant, not the product formation rate constant as assumed by Freyer, because transition state theory assumes equilibrium between the stable *reactants* and the transition state [*Bigeleisen and Wolfsberg*, 1958; *Wolfsberg et al.*, 2010]. In other words, Freyer's $\alpha = 0.9971$ should indicate that the $^{15}NO_2$-OH decomposes more slowly than $^{14}NO_2$-OH and therefore more likely to form HNO_3 at +2.9‰ (not -2.9‰ determined in Freyer). Secondly, the reduced mass approximation of the complex pair ignores the thermodynamic contribution of the reactants and the vibrations in the transitions state other than the bond forming (imaginary) vibration. Our approach overcomes both of these assumptions and incorporates the temperature dependence of the EIE for this reaction.

2.4.3.3 EIE used in heterogeneous reactions of N_2O_5

During the nighttime, the heterogeneous HNO_3 formation pathway becomes important [*Chang et al., 2011; Dentener and Crutzen, 1993; Riemer et al., 2003*]. During the night, NO is nearly completely oxidized to NO_2 leading to the build-up of the NO_3 radical (R48), the formation of N_2O_5 (R53), and heterogeneous N_2O_5 hydrolysis becomes a major source of HNO_3 production (discussed below). This is particularly true in regions that have high NO_x mixing ratios and large aerosol surface areas such as urban centers [*Chang et al., 2011; Riemer et al., 2003*]. In order to assess the ^{15}N partitioning of this reaction pathway, both EIE and KIE were considered.
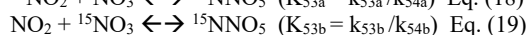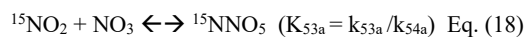
It was assumed that the fractionation factor for the $N_2O_5 \rightarrow 2HNO_3$ reaction was mainly controlled by nighttime equilibrium between N_2O_5 and NO_2/NO_3 (R53, R54). When factoring the isotopologue dynamics, this equilibrium can be viewed as an EIE via

$^{15}NO_2 + NO_3 \leftrightarrow O_2{}^{15}N\text{-}O\text{-}NO_2 \leftrightarrow NO_2 + {}^{15}NO_3$ Eq. (17)
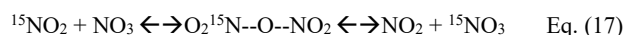
here $^{15}N_2O_5$ is represented as the transition state $O_2{}^{15}N$-O-NO_2 to highlight the relative ease of N isotope exchange via oxygen migration during N_2O_5 formation and decomposition. The symmetry of $^{15}NNO_5$ and $N^{15}NO_5$ is also why they were not treated as isotopomers since they are structurally identical.

13
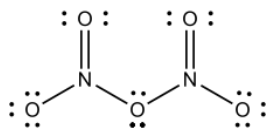
The N_2O_5 equilibrium in the RACM model is dealt with as a forward reaction R53 (k_{53}) and a decomposition reaction R54 (k_{54}) that are derived from the measured equilibrium constant (K_{53}) = (k_{53}/k_{54}). In i_NRACM the N_2O_5 isotopologue has 2 formation pathways, with two forward rate constants ($k_{53\,a,b}$) and two decomposition rate constants ($k_{54\,a,b}$) that were used to write their respective equilibrium constants K

$^{15}NO_2 + NO_3 \longleftrightarrow {}^{15}NNO_5$ ($K_{53a} = k_{53a}/k_{54a}$) Eq. (18)
$NO_2 + {}^{15}NO_3 \longleftrightarrow {}^{15}NNO_5$ ($K_{53b} = k_{53b}/k_{54b}$) Eq. (19)

Dividing K_{53a} and K_{53b} by K_{53} yields isotopologue product and reactant ratios that can be evaluated using $\beta(\alpha)$ values from Walters and Michalski (*2015*). These were used to determine the α value for the N_2O_5 isotopologue equilibrium, which are simply a function of the formation and decomposition rate constants and temperature

$K_{53a}/K_{53} = ({}^{15}NNO_5/N_2O_5)(NO_2/{}^{15}NO_2)(NO_3/NO_3) = \beta_{N2O5}/\beta_{NO2}$
$= \alpha_{N2O5/NO2} = k_{53a}/k_{53} \times k_{54}/k_{54a}$ Eq. (20)
$K_{53b}/K_{53} = ({}^{15}NNO_5/N_2O_5)(NO_3/{}^{15}NO_3)(NO_2/NO_2) = \beta_{N2O5}/\beta_{NO3}$
$= \alpha_{N2O5/NO3} = k_{53b}/k_{53} \times k_{54}/k_{54b}$ Eq. (21)

The N_2O_5 decomposition rate constants were arbitrarily set to be equal ($k_{54} = k_{54a} = k_{54b}$) and the decomposition rate constants were then derived using the temperature dependent α values

$k_{53a} = k_{53}(\alpha_{N2O5/NO2})$ $\alpha_{N2O5/NO2} = 1.0266$ (298 K) Eq. (22)
$k_{53b} = k_{53}(\alpha_{N2O5/NO3})$ $\alpha_{N2O5/NO3} = 1.0309$ (298 K) Eq. (23)

The α for doubly substituted $^{15}N_2O_5$ isotopologue was determined using $\alpha = \beta_{15N2O5}/\beta_{NO2}\beta_{NO3}$ and the value for β_{15N2O5} (1.272) was approximated using the principle of the geometric mean [*Bigeleisen*, 1958; *Snyder et al.*, 1999], yielding a temperature independent $\alpha = 1.057$. However, the N_2O_5 system is insensitive to this α value because the low probability of a $^{15}N + {}^{15}N$ reaction (1.5×10^{-5}) relative to a $^{14}N + {}^{15}N$ reaction (4×10^{-3}), thus the small temperature dependence was also ignored.

Because RACM is a gas phase chemical mechanism, it does not include heterogeneous reactions of N_2O_5 on aerosols, which would limit i_NRACM to accurately predict the $\delta^{15}N$ values, particularly at night. Gas chemical mechanisms are often used in larger 1, 2, and 3-D chemical transport models that usually also include aerosol modules that calculate heterogeneous chemistry using inputs from the gas phase chemical mechanism (i.e. N_2O_5 concentrations). However, if the objective is to use a 0-D chemical box model to simulate local chemistry the N_2O_5 heterogeneous hydrolysis will need to be included. i_NRACM was modified to use a first order rate constant to calculate N_2O_5 heterogeneous hydrolysis [*Yvon et al. 1996; Riemer et al., 2003*]. The rate constant is a function of N_2O_5 molecular speed (c), the N_2O_5 uptake coefficient (γ) and the aerosol surface area density S.

$-dN_2O_5/dt = d0.5HNO_3/dt = k_{N2O5}[N_2O_5] = R239$ $k_{N2O5} = \frac{1}{4}c \gamma S$ Eq. (24)

The k_{N2O5} values were assessed based on the different pollutant loadings and emission scenarios (Fig. 6). The k_{N2O5} was calculated as a function of γ *[Anttila et al, 2006; Bertram & Thornton. 2009; Davis et al., 2008; Riemer et al., 2003; Riemer et al., 2009]* and S *[Cai et al., 2018; Kuang et al., 2010; McMurry et al., 2005; Petäjä et al., 2009; Qi et al., 2015]* values that span clean to highly polluted environments. This range yielded k_{N2O5} = 1, 0.1, and 0.01 for high, medium, and low polluted environments (Fig. 6).

Only the uptake coefficient (γ) and molecular speed (c) could have a KIE during aerosol uptake of N_2O_5 (R239, R239a, R239b). The γ term was ignored because *ab initio* work suggests that N_2O_5 hydrolysis activates through hydrogen bonding between water molecules on the aerosol surface and O atom in the N_2O_5 *[Snyder et al., 1999]* making it a secondary (small) KIE for N. The c term is a function of the root of the N_2O_5 molecular mass and when the ratio is taken there is no temperature dependence yielding $\alpha_{239a} = (108/109)^{0.5} = 0.995$ and $\alpha_{239b} = (108/110)^{0.5} = 0.9909$.

Figure 6. Contour lines of the same k_{N2O5} values as a function of γ and S values. The γ values depend on aerosol composition and range from 3.8×10^{-5} (relatively dry sulfuric acid) to 1 (aqueous aerosol in the winter polar stratosphere). S values are a function of aerosol number density and size distribution and range from 52 (low scavenging rate, low particle growth rate) to 1140.1 (high scavenging rate, high particle growth rate).

An online version of this i_NRACM model is available for public use at
https://mygeohub.org/tools/sbox/

2.4.4 i_NRACM simulations

A number of i_NRACM simulations were run with two different purposes. The first set of simulations iteratively changed the α values from 1 to their values discussed above. These simulations aimed at investigating the importance of each α as they aggregated together. These include photolysis only, Leighton cycle, daytime chemistry, night-time chemistry, and full chemistry using the same test case (Table S3a-f). These were run with all α's activated but with varied initialized chemistry and primary pollutant emissions.

Deleted: The second set of simulations replicated the test case simulations (Table S4a-b, 5a-b) detailed in Stockwell (1997) and other pollution scenarios (Table S8).

3.0 Results and Discussion

It is important to first test i_NRACM by turning on and off individual relevant isotope effects and then combining their cumulative effects. This is advantageous relative to simply running the full mechanism under different pollution scenarios because it would be a challenge to disentangle which isotope effects in the full mechanism were mainly responsible for $\delta^{15}N$ change in NO_x, HONO, or HNO_3 without such a systematic investigation. For example, it is likely that the $\delta^{15}N$ value of NO_2 will be a significant factor in the $\delta^{15}N$ value of HNO_3 because it is the reactant in
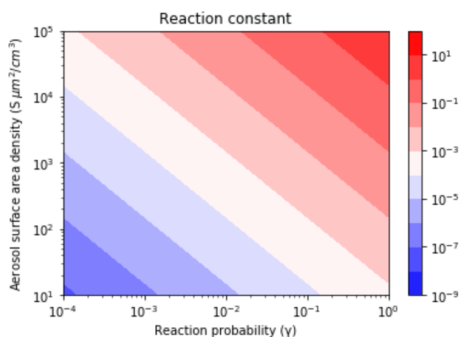
15

R39 and R239. Thus, understanding which isotope effects control the $\delta^{15}N$ of NO_2 helps with interpreting the $\delta^{15}N$ value of HNO_3 and vice versa. Thus, this discussion section is divided into 3 sections. The first is the examination of the relevant isotope effects occurring during daytime photochemistry and their impact on NO_x, HONO, and HNO_3 $\delta^{15}N$ values. Secondly, is the examination of the relevant isotope effects occurring during nighttime chemistry (EIE and KIE) and their effect on NO_x, HONO, and HNO_3 $\delta^{15}N$ values. These first two discussion sections focus mainly on the relative importance of each isotope effect when the photochemical conditions are constant. Finally, the full i_NRACM mechanism will be tested under different atmospheric conditions such as variations in trace gas concentrations, aerosol loading, and hours of sunlight. This tests how changes in photochemical oxidation pathways results in difference in the $\delta^{15}N$ values of NO_x, HONO, and HNO_3.

3.1 The $\delta^{15}N$ of NO_x, HONO, and HNO_3 due to daytime chemistry

The role that daytime chemistry plays in determining the $\delta^{15}N$ values of NO_x, HONO, and HNO_3 was investigated by iteratively adding relevant fractionation factors to i_NRACM. The sensitivity of NO_x, HONO, and HNO_3 $\delta^{15}N$ values to NO_2 photolysis (R1a) was tested. The initial trace gas concentrations and emissions were set to the March 1 test cases (Table S3 a-f) and simulations were run with, and without, NO emissions. All subsequent test simulations will also use the March 1 test case in order to have a consistent comparison of $\delta^{15}N$ values between different simulations. It is noted that the initial HNO_3 and O_3 mixing ratios are set to zero and that the start time of the simulations is 3 a.m. The main daytime only effects will be NO_2 photolysis (R1), O_3 oxidation (R8) and reaction OH (R39) since both photolysis and OH chemistry is only relevant during the daytime. However, NO_x isotope exchange and $NO + O_3$ will also play a vital role despite no being exclusively daytime reactions.

3.1.1 The $\delta^{15}N$ values of NO_x, HONO, and HNO_3 due to the photolysis only
The simulations with only R1 isotope effect activated (with NO_x emissions) shows a clear diurnal cycle in NO_x and HONO $\delta^{15}N$ values and a multiday trend moving towards an approximate steady state for HNO_3 $\delta^{15}N$ values, which can be explained by the PHIFE (Fig. 7a). Initially all NO_y has $\delta^{15}N$ of zero (by default) and there is no photolysis at 3 am. At sunrise the $\delta^{15}N$ value of NO_2 goes negative and NO value positive since $^{15}NO_2$ is preferentially photolyzed ($\alpha_{R1} = 1.0042$).

The difference between the $\delta^{15}N$ values of NO and NO_2 ($\Delta\delta^{15}N_{NO-NO2} = \delta^{15}N$ NO - $\delta^{15}N$ NO_2) at all times during the day is 4‰, which is the ε_{R1a} value. During the night both the NO and NO_2 $\delta^{15}N$ values approach 0‰ because most NO is oxidized to NO_2 and NO emissions (0‰) dominate the NO nighttime budget (relative to residual day NO). Over the weeklong simulation, the NO_x $\delta^{15}N$ value slowly increases by about one per mil. This is because ^{15}N depleted NO_2 is converted into HNO_3 leaving the residual NO_x ^{15}N enriched. This is also the reason for the $\delta^{15}N$ values of HNO_3 that initially mimic the daytime NO_2 values and trends towards 0‰ by the end of the simulation week. The $\delta^{15}N$ values of HONO mimics the NO values during the daytime since the main reaction pathway forming HONO is OH + NO, which peaks in the morning (~10:00). HONO retains the evening $\delta^{15}N$ values through the night since most of the HONO is destroyed in the afternoon via photolysis and again follows NO
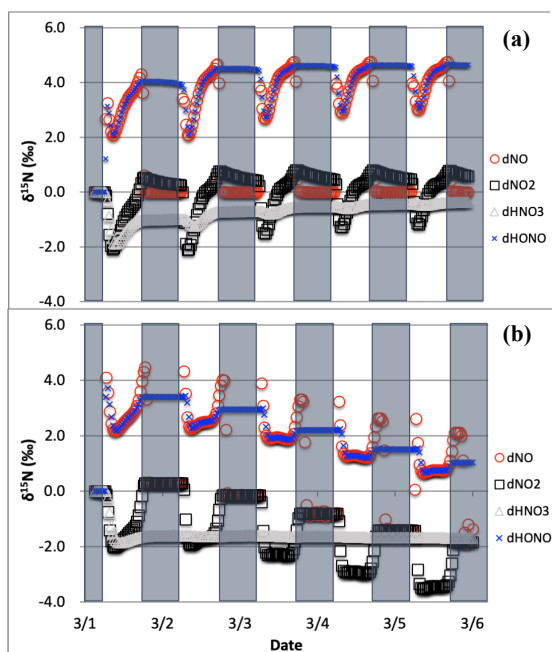

Figure 7. The $\delta^{15}N$ values of NO (O), NO_2, (□) HONO (x), and HNO_3 ( ) with only the photolysis isotope fractionations active. The 5-day simulation was under the conditions list in Table S3a-b. The gray boxes span night hours and the white span daytime. The top (a) is the simulation with NO_x emissions and the bottom (b) is without NO_x emissions.

$\delta^{15}N$ the next morning as its production again reaches a maximum (Fig. 7a).

The simulation without NO emissions shows a similar behavior but with some clear differences relative to the emission case. The NO_x and HONO $\delta^{15}N$ values exhibit the same diurnal $\Delta\delta^{15}N_{NO-NO2} = 4$‰ value. Unlike the emission case, however, the diurnal NO_x $\delta^{15}N$ value peaks and troughs trend downward during the week-long simulation, with NO approaching 0‰ and NO_2 approaching -4‰. The HNO_3 $\delta^{15}N$ values reach roughly a steady state value of -1.7‰ after about a day and NO_x is ~ -1.8‰ (Fig. 7b). This difference between the emission and non-emission case is a consequence of isotope mass balance (f_x = mole fraction of compound x relative to total NO_y).

$$\delta^{15}N_{total} = 0 = f_{NOx} \bullet \delta^{15}N_{NOx} + f_{HNO3} \bullet \delta^{15}N_{NHNO3} + f_{ONIT} \bullet \delta^{15}N_{ONIT} \qquad \text{Eq. (25)}$$

The positive $\delta^{15}N$ NO_y compound that effectively offsets the -1.7‰ in HNO_3 and -1.8‰ in NO_x is organic nitrate that is +2‰ and makes about half the NO_y pool and is roughly equal to HNO_3 + NO_x ($f_{NOx} = 0.11$, $f_{HNO3} = 0.36$, $f_{ONIT} = 0.53$). In the NO_x emission case only about 5% of NO_y is as organic nitrate ($f_{NOx} = 0.17$, $f_{HNO3} = 0.78$, $f_{ONIT} = 0.05$) indicating a shift in oxidation pathways when NO and VOCs are emitted during the simulation relative to when they are not. In the emissions case the NO_x mixing ratios at the end of the simulation are actually slightly higher than their initial ratios, in contrast to the no NO_x emission case where 90% of NO_x has been lost via oxidization into organic nitrate and HNO_3. This loss of N in the no emission scenario effectively shuts down the oxidation chemistry. For example, the day 5 mixing ratio of O_3 is 45 ppb_v (reasonable) for the emission case but only 2 ppb_v for the non-emission case (unreasonable). Therefore, we exclude no-emission simulations for the chemistry analysis discussed in this section and restrict them to the no emission simulations to 48 hours in the final test case analysis (See section 4).
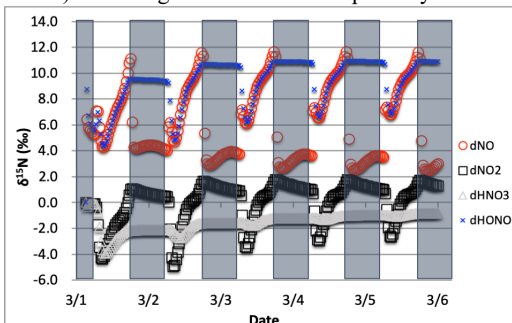
Figure 8. The $\delta^{15}N$ values of NO_x, HONO, and HNO_3 when isotope effects associated R1 and R48 are combined, with NO_x emission. The 5-day simulation was under the conditions list in Table S3a-b. The diurnal patterns are reflecting the relative importance of photolysis and O_3 chemistry during the day and night.

3.1.2 The $\delta^{15}N$ values of NO_x, HONO, and HNO_3 due to the combined Leighton cycle

The simulations with both NO_2 photolysis (R1) and O_3 + NO (R48) isotope effects active shows similar diurnal and multiday trends as the photolysis only simulations, they are just slightly amplified (Fig. 8). The daytime $\Delta\delta^{15}N_{NO-NO2}$ is now ~ 9.5‰, which is close to the additive of the two isotope effects ($\epsilon_{48a} = -6.7‰$, $\epsilon_{R1a} = 4.2‰$). This is logical since ^{15}NO is reacting with O_3 slower than ^{14}NO, preferentially leaving behind ^{15}NO and thus the higher NO $\delta^{15}N$ value. The HNO_3 $\delta^{15}N$ values reach the mean of the daytime NO_2 $\delta^{15}N$ values via the NO_2 + OH reaction. The slight (1‰) upward trend of NO_x and HNO_3 are due to isotope mass balance as detailed in the photolysis only case. Similar to the photolysis only case the $\delta^{15}N$ of HONO is mimicking daytime NO $\delta^{15}N$ values.

3.1.3 The $\delta^{15}N$ values of NO_x, HONO, and HNO_3 due to the combined Leighton cycle and NO_x isotope exchange

The $\delta^{15}N$ values of NO_x produced when both the Leighton cycle and NO_x isotope exchange are active exhibit a very dynamic diurnal range that is a function of the NO_x mixing ratios. At high NO_x mixing ratios (150 ppb, 1/3 NO, 2/3 NO_2, Fig. 9a) the $\Delta\delta^{15}N_{NO-NO2}$ is -40‰ at night as expected for NO_x isotopic equilibrium ($\epsilon_{NO/NO2} = -40‰$ at 298K). During the daytime the $\Delta\delta^{15}N_{NOx}$ shifts -30 to -35‰ as the photolysis and O_3 isotope effects begin to influence the $\Delta\delta^{15}N_{NO-NO2}$. HNO_3 $\delta^{15}N$ values during the high NO_x mixing ratio simulation initially follow the $\delta^{15}N$ of NO_2 (via NO_2 + OH) before approaching 0‰, the defined NO_x source values.

18

At low NO$_x$ mixing ratios (1.5 ppb, 1/3 NO, 2/3 NO$_2$, Fig. 9c) the $\Delta\delta^{15}N_{NO-NO2}$ and HNO$_3$ $\delta^{15}N$ is very different from the high NO$_x$ simulation. The nighttime $\Delta\delta^{15}N_{NO-NO2}$ ranges from -15 to -20‰ and during the daytime it is around +7‰, while the HNO$_3$ $\delta^{15}N$ values hover around zero throughout the simulation. The difference between the NO$_y$ $\delta^{15}N$ values in the high and low NO$_x$ cases can be explained as a competition between the NO$_x$ EIE and the Leighton isotope effect. At high NO$_x$ mixing ratios, the NO$_x$ EIE achieves equilibrium quickly at night ($\Delta\delta^{15}N_{NO-NO2}$ = -40) because the rate of NO$_x$ isotope exchange (R238) is proportional to its concentration. In contrast, isotope exchange is slow in the low NO$_x$ case and the time scale to reach equilibrium is much longer. Indeed, at the low NO$_x$ mixing ratios the nighttime equilibrium only reaches about 40-50% of completion by 6:30. Afterwards sunlight begins to erase the NO$_x$ EIE effect until around noon when the $\delta^{15}N$ values of NO is mostly due to the Leighton effect and only a small contribution from EIE (about 5%). For intermediate NO$_x$ mixing ratio case (15 ppb, 1/3 NO, 2/3 NO$_2$, Fig. 9b) the diurnal and week-long NO$_y$ $\delta^{15}N$ trends fall somewhere in between the high and low NO$_x$ simulations.

The changes in $\delta^{15}N$ values of HNO$_3$ during the March 1 simulations at differing NO$_x$ mixing ratios can be explained in terms of HNO$_3$ production pathways. Over the course of day 1 the $\delta^{15}N$ of HNO$_3$ mirrors that of NO$_2$ because HNO$_3$ produced by NO$_2$ + OH (R39), thus the product HNO$_3$ $\delta^{15}N$ values are similar to those in NO$_2$. This varies depending on the NO$_x$ mixing ratio scenario for two reasons. First, as the NO$_x$ mixing ratio gets bigger, the closer the NO$_x$ gets to achieving the EIE and the bigger the split between NO and NO$_2$ $\delta^{15}N$ values (40‰ versus 10‰ for Leighton+O$_3$). Secondly,
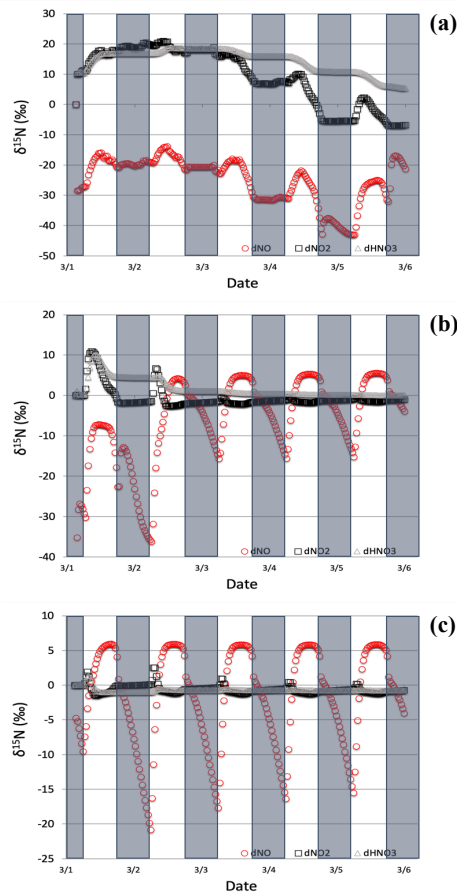

Figure 9. The $\delta^{15}N$ values of NO$_x$ and HNO$_3$ when isotope effects in R1, R48, and R238 are included under high (top, a), medium (middle, b), and low (bottom, c) NO$_x$ scenarios. The 5-day simulation was under the conditions list in Table S3d-f. The NO$_y$ $\delta^{15}N$ values are mainly controlled by NO$_x$ isotope exchange (R238) under high NO$_x$ conditions and Leighton (R1 + R58) under low NO$_x$ conditions.

differences in the amount of NO$_x$ result in different NO/NO$_2$ ratios as the simulations progress. For example, under low NO$_x$ mixing ratios the nighttime NO/NO$_2$ < .001, which means the $\delta^{15}N$ value of NO$_2$ will be close to that of total NO$_x$, which will be close to 0‰. At the same time the

$\delta^{15}N$ value of NO will be close to the fraction of the EIE achieved, which is about 50% under low NO_x conditions, resulting in a NO $\delta^{15}N$ of about -15‰. These two effects control the $\delta^{15}N$ of NO_2 and that in turn controls the $\delta^{15}N$ value of HNO_3. In all scenarios the diurnal cycle repeats itself over the subsequent 4 days and a greater fraction of total NO emitted has been turned into HNO_3, so that by the end of the 5-day simulation the HNO_3 $\delta^{15}N$ values converge towards 0‰, the defined value of NO_x emissions in the simulations.

The modeled $\delta^{15}N$ values of HONO also have a diurnal pattern that can also be traced to diurnal chemistry and isotope mass balance. Similar to the photolysis and photolysis + O_3 cases, the HONO $\delta^{15}N$ values mirror the oscillation of the NO $\delta^{15}N$ values (data no shown). This is a result of HONO production by the NO + OH reaction (R38). In contrast, the HONO $\delta^{15}N$ values at night remain nearly constant despite the fact that the $\delta^{15}N$ of NO is changing dramatically. This is because the absence of OH at night halts R38 and thus HONO production ceases and the $\delta^{15}N$ values are simply the same as the residual daytime HONO reservoir. There is a repeated minimum in HONO $\delta^{15}N$ values occurring each morning at 7:00 over the subsequent 4 days. This is a result of the fact that, unlike HNO_3, HONO is effectively destroyed by photolysis (R4) and OH (R45). Thus, HONO does not build up in the model over the 5-day simulation, but rather mixing ratio peaks daily (30 ppb) at around 9:00 each day. This is when the HONO production – destruction rate is greatest, and its mixing ratio then deceases to a low of 2 ppt by sunset. Since the nighttime

HONO, with $\delta^{15}N$ ~ +5.5‰, only contributes about 7% ($f = 0.07$) of the morning HONO spike, it does not greatly impact the control that NO $\delta^{15}N$ has on the HONO $\delta^{15}N$ value. This daily isotope effect should be contrasted with the HNO_3 $\delta^{15}N$ trends with time. Initially HNO_3 $\delta^{15}N$ values are influenced by NO_2 $\delta^{15}N$ variations by NO_2-OH-HNO_3 coupling, similar to the NO-OH-HONO coupling. But since there is no significant photochemical sink of HNO_3, the control on HNO_3 $\delta^{15}N$ values by HNO_3 accumulation increases with time, so that by day 5 the diurnal changes in NO_2 $\delta^{15}N$ have almost no impact on the HNO_3 $\delta^{15}N$ values (Fig. 9).
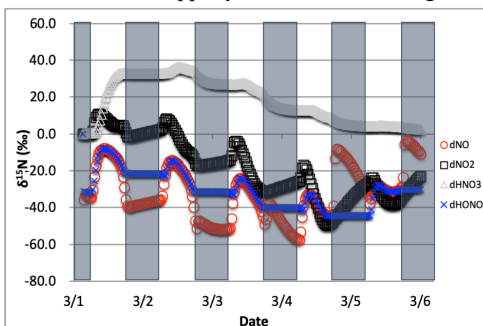

Figure 10. The time evolution of $\delta^{15}N$ values of NO, NO_2, HNO_3, and HONO caused by isotope effects of Leighton reactions, NO_x isotope exchange, and NO_2 + OH reaction, with NO emission, simulation starts from Mar 1. The 5-day simulation was under the conditions list in Table S3c.

3.1.4 The $\delta^{15}N$ values of NO_x, HONO, and HNO_3 due to the combined Leighton cycle, NO_x isotope exchange, and NO_2 + OH

The effect of the NO_2 + OH reaction has on $\delta^{15}N$ values of NO_x and HNO_3 associated was then examined (Table S3c). Since R39 is the last step in HNO_3 production, the instantaneous $\delta^{15}N$ $HNO_3 = \delta^{15}N(NO_2) + \varepsilon_{39}$, thus the $\delta^{15}N_{HNO3}$ is initially 40‰ higher than the NO_2 (Fig. 10). This in turn depletes ^{15}N in the residual NO_2 leading to more negative $\delta^{15}N$ values in NO_2 relative to the Leighton + exchange simulations (Fig. 10). These latter two effects are still in play as evident by the diurnal NO_x $\delta^{15}N$ cycling and $\Delta\delta^{15}N_{NO-NO2}$. As the 5-day simulation progresses, the HNO_3

$\delta^{15}N$ value approaches 0‰, approaching the $\delta^{15}N$ of NO emissions, as expected based on isotope mass balance. We point out that this convergence to the source NO_x $\delta^{15}N$ value is much slower in this case than the Leighton and exchanges cases. This highlights the importance of the knowing the correct ε_{48}. If $\varepsilon_{39} \sim 0$ as suggested by Freyer (1991) then daytime the $\delta^{15}N$ $HNO_3 \cong \delta^{15}N$ NO_2, demonstrably lower than the $\varepsilon_{39} \sim 40‰$ case. In the end the average daytime $\delta^{15}N$ value of HNO_3 for the entire simulation is about 10‰ higher than the $\delta^{15}N$ of the NO_x source (here defined as 0‰).

3.2 The $\delta^{15}N$ values of NO_x, HONO, and HNO_3 due to nighttime chemistry

The role that nighttime chemistry plays in determining the $\delta^{15}N$ values of NO_x, HONO, and HNO_3 was investigated by iteratively adding relevant fractionation factors to iRACM. The nighttime chemistry effect was assessed by separating the effects of NO_3 radical chemistry and N_2O_5 heterogeneous hydrolysis. NO_3 radical chemistry is only relevant at night because of its short daytime lifetime with respect to photolysis, which keeps its daytime mixing ratios at the sub ppt_v levels [*Platt et al., 1984*]. At night NO_3 builds up and produces HNO_3 [*Aldener et al., 2006; Finlayson-Pitts and Pitts, 1997; Horowitz et al., 1998*] via reactions with hydrocarbons (R91-97). The magnitude of this isotope effect was tested by adding NO_3 the isotope fractionation factors for R91-97 (see methods) and altering VOC emission rates to simulate clean, moderate, and extreme VOC pollution environments. Likewise, N_2O_5 only accumulates at night when it begins producing HNO_3 on aerosol surfaces [*Chang et al., 2011*]. The magnitude of this isotope effect was tested by adding the N_2O_5 EIE (see methods) and adding the first order N_2O_5 heterogeneous pathway (see methods) to i_NRACM. The first-order rate constant was adjusted to simulate clean, polluted, and extreme pollution environments where aerosol surface area density largely controls the rate constant [*Riemer et al., 2003 Chang et al., 2011*].
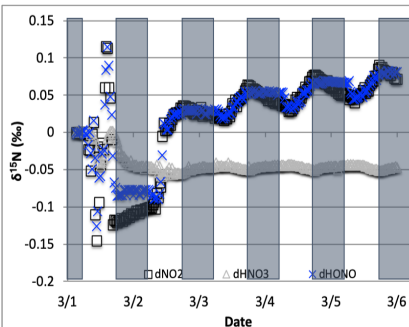

Figure 11. The difference between the $\delta^{15}N$ values of NO_2, HONO, and HNO_3 when NO_3 + VOC → HNO_3 reactions are included and excluded (NO was omitted for clarity). The 5-day simulation was under the conditions list in Table S3e. Total VOC mixing ratios during the last day of the March 1 simulation was 550-670 ppb C.

3.2.1 The $\delta^{15}N$ values of NO_x, HONO, and HNO_3 due to NO_3 + VOC reactions

The effect on the $\delta^{15}N$ values of NO_x, HNO_3, HONO associated with the KIE occurring during NO_3 + VOC nighttime reactions (R91-R97) were first examined. Four simulations were run that included the isotope effects (α values in Table S4) of the Leighton cycle (R1 and R48), NO_x

isotope exchange (R238), NO_2 + OH production of HNO_3 (R39), and the KIE effects (R91-R97), as well as NO emissions. The simulation tested first was the March test case (medium VOC ~360 ppb_v). Then, two simulations were run for June 1 (extended sunlight, warm temperatures), one with high initial of VOC concentrations and a high VOC emission rate (2 ppb_v h^{-1}) and one with low emission rate of VOCs (0.4 ppb_v h^{-1}). The same two initial conditions were used in the Jan. 1 test case to assess if the extended nighttime and cold temperatures significantly affected the NO_x of HNO_3 $\delta^{15}N$ values produced by NO_3 radicals. The impact of NO_3 reactions on NO_y $\delta^{15}N$ values was determined by subtracting these simulated $\delta^{15}N$ values from those same simulations when only the Leighton cycle, exchange and OH + NO_2 reaction was considered (Section 3.1).

Figure 12. The difference in $\delta^{15}N(HNO_3)$ values when NO_3 + VOC $\rightarrow$ HNO_3 reactions are included and excluded, for Mar 1 simulation, relative to Jun 1 simulation (□) and Jan 1 simulation (o). The 5-day simulation was under the conditions list in Table S3e.

The NO_3 + VOC KIE induced a minor diurnal pattern on the $\delta^{15}N$ values of NO_x, and HONO, and a trend for HNO_3 for the March test case, but the size of the effect was relatively small (e.g., < 0.4‰; Fig. 11). At the start of the simulation (3 am) there is no HNO_3, therefore the initial HNO_3 is produced via OH production of HNO_3 (R39),

$\delta^{15}N$ values of HNO_3 decreased from 0.35 to 0.2‰ during the night. The pattern is because of increasing the importance of R91-R97 in HNO_3 production at night. The smallness of the effect is because α values are all relatively small, the average δ for the NO_3 + VOC is about -4‰, and the relatively small amount of HNO_3 produced via these pathways (around 2.6 % of 24-hour HNO_3). The first source of the HNO_3 in the simulation (3 to 6 am) is the NO_3 + VOC reactions and results in a slight negative $\delta^{15}N$ in HNO_3 value (-0.01‰). This leaves the residual NO_3^- ^{15}N enriched that is then photolyzed into NO_2 at sunrise and used NO_2 + OH $\rightarrow$ HNO_3 production resulting in slight positive $\delta^{15}N$ values (+0.35‰) (Fig. 11). The range of the diurnal HNO_3 $\delta^{15}N$ oscillation dampens as the fraction of emitted NO that has been converted to HNO_3 has increased over time. The diurnal and multiday change in $\delta^{15}N$ of HNO_3 changes did not significantly change during the winter and summer simulations (Fig. 12) run with and without the KIE for R91-R97 show negligible differences, similar to those in Fig. 11. In conclusion, although there is some $\delta^{15}N$ effect

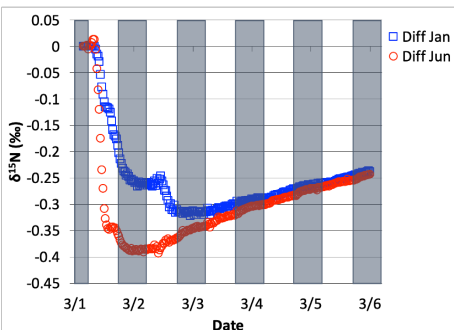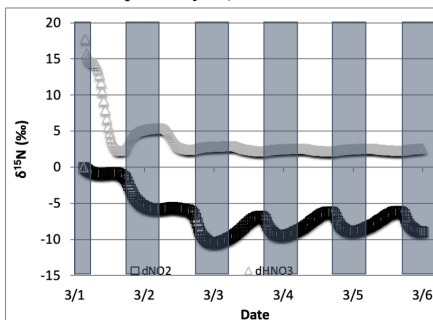Figure 13. The difference in $\delta^{15}N$ values of NO_2 and HNO_3 when the isotopic effect during N_2O_5 heterogeneous reactions (R53-54, R239) is included (α_{N2O5} =1.029) and when it is excluded (α_{N2O5} = 1.0). The 5-day simulation was under the conditions list in Table S3e.

associated with NO_3 + VOC chemistry, it is much smaller than the effects associated with the Leighton cycle, NO_2 + OH, and NO_x equilibrium.

3.2.2 The $\delta^{15}N$ values of NO_x, HONO, and HNO_3 due to N_2O_5 reactions

The effect on the $\delta^{15}N$ values of NO_x, HNO_3, HONO associated with the EIE of N_2O_5 heterogeneous hydrolysis was also tested. March 1 simulations with N emissions and $k_{N2O5} = 0.1$ s^{-1} were run that included the isotope effects of the Leighton cycle (R1 and R48), NO_x isotope exchange (R238), OH production of HNO_3 (R39), and the N_2O_5 EIE (R53-54) KIE (R239) (Table S5), as well as NO emissions. These simulations were compared to an identical simulation but where the α_{N2O5} was set equal to 1.0. This ensured that the NO_y chemistry was not altered when comparing the two simulations (i.e., $\alpha_{N2O5} = 1.029$ vs. $\alpha_{N2O5} = 1.0$). The effect of N_2O_5 chemistry on the $\delta^{15}N$ values of NO_2 and HNO_3 was investigated. Similar to the March 1 NO_3 + VOC tests, simulations with R1, R39, R48, R238, and R239 isotope effects active were run and then compared to simulations with the same conditions but with R239 turned off. In addition, March simulations were run using three different k_{N2O5} values (.01, 0.1 and 1) and compared to each other in order to test the range of NO_2 and HNO_3 $\delta^{15}N$ values that could be generated solely by heterogeneous N_2O_5 hydrolysis.

The average daily $\delta^{15}N$ values of HNO_3 exhibit some diurnal oscillations that roughly reach a steady state average value after simulation day 2. At that point HNO_3 has a $\delta^{15}N = +2.5‰$ relative to the $\alpha_{N2O5} = 1.0$ simulation. In contrast the NO_2 $\delta^{15}N$ values oscillate diurnally by about +/- 2‰ around an average daily difference of about -8‰. This change is due to the R53-54 equilibrium, which predicts ^{15}N enrichment in N_2O_5 (and thus HNO_3) and depletion in NO_3 and NO_2. The N_2O_5 produces HNO_3 with the highest $\delta^{15}N$ difference (~ +29‰) during the first simulation morning. This is because all of the initial HNO_3 is produced by N_2O_5 due to the 3 am simulation start time. The roughly steady state HNO_3 $\delta^{15}N$ value of +2.5‰ is a consequence of the fact that when $\alpha_{N2O5} = 1.0$ HNO_3 is being produced by N_2O_5 at 0‰ and when $\alpha_{N2O5} = 1.029$ it is being produced at +29‰. The ratio of this simulated +2.5‰ value and N_2O_5 enrichment factor of +29‰ yields 0.086, the fraction of HNO_3 produced by N_2O_5. This is similar to the

Figure 14. The difference in $\delta^{15}N(HNO_3)$ values when the isotopic effect during N_2O_5 heterogeneous reactions is included and when it is excluded, for the simulation of $k_{N2O5} = 0.1$, relative to 0.01 (□) and 1.0 (o). The 5-day simulation was under the conditions list in Table S3e.

fraction of HNO_3 produced in simulations when the N_2O_5 reaction was active and where it is inactive, which yielded a fraction of 0.064. The difference in these fractions is because deactivating N_2O_5 chemistry changes overall NO_y chemistry and HNO_3 production *[Dentener and Crutzen, 1990]*.

The effect of N_2O_5 chemistry on the $\delta^{15}N$ values of NO_2 is more dynamic than HNO_3 (Fig. 13). This is mainly due to the fact that HNO_3 is continually building up over time and thus its

Deleted: 7

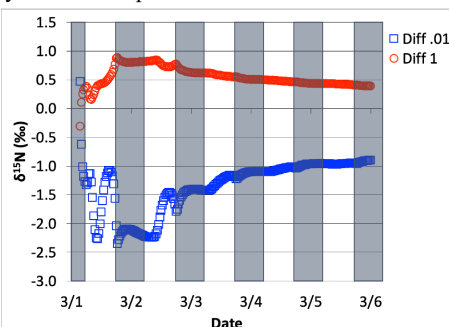$\delta^{15}N$ is less susceptible to change by small additions. The oscillation in the NO_2 $\delta^{15}N$ value becomes more negative at night, which corresponds to the increase in the HNO_3 $\delta^{15}N$ values. This is a reflection of ^{15}N preferentially incorporating into N_2O_5 resulting in NO_2 depleted in ^{15}N. Similar oscillations are found in NO and HONO (data not shown) as they are connected to NO_2 build-up and decay diurnally. This suggests that night-time partitioning of NO_y will have a small but measurable influence on daytime NO_y $\delta^{15}N$ values. The effect of using different k_{N2O5} values had a small but measurable effect on the NO_2 and HNO_3 $\delta^{15}N$ values. Simulations that used a k_{N2O5} = 1.0 resulted in HNO_3 $\delta^{15}N$ values that were about 2‰ lower than those run at k_{N2O5} = 0.01 and 1‰ heavier than when k_{N2O5} = 1.0. This makes sense because the mean EIE for N_2O_5 (29‰) is lower than that for $NO_2 + OH$ (40‰), therefore as N_2O_5 produces more HNO_3 its $\delta^{15}N$ value would decrease with respect to that of daytime HNO_3 production. Thus, the model predicts lower HNO_3 $\delta^{15}N$ values in cold, dark polluted regions (relative to the tropics where) where N_2O_5 heterogeneous hydrolysis may be the main HNO_3 production pathway *[Dentener and Crutzen, 1990]*.

3.3 Assessing i_NRACM's ability to predict in particulate NO_3^-

There are a number of challenges when trying to compare the i_NRACM model predictions of NO_y $\delta^{15}N$ values with observations in real world. First, there has yet to be a study where the $\delta^{15}N$ values of NO, NO_2, and NO_3^- have been simultaneously measured. The most abundant data is on the $\delta^{15}N$ value of NO_3^- in aerosols or rainwater. Even with these studies, a direct comparison is difficult because of the $\delta^{15}N$ value of the source NO_x may be variable in space and time. The $\delta^{15}N$ value of NO_x sources can range from -40 to + 20 ‰ and both NO_x sources and NO_3^- deposition will be a strong function of the transport history of the air mass that is sampled. Without a 3-D chemical transport model that includes the i_NRACM mechanism, a direct comparison with most NO_3^- $\delta^{15}N$ studies would be tenuous. In addition, most NO_y $\delta^{15}N$ studies provide neither trace gas concentrations (NO_x, O_3, CO, VOC) nor local trace gas emissions that would be required to constrain i_NRACM for it make an accurate prediction of secondary pollutants or $\delta^{15}N$ values.

The most complete dataset for which to evaluate the i_NRACM mechanism is from Riha (2013) in a study in Tucson AZ, USA. In that study $PM_{2.5}$ and PM_{10} were collected weekly (24-hour period) for one year (2006) and the $\delta^{15}N$ value of water soluble NO_3^- from was determined (Fig. 15). It contains PM mass and NO_3^- $\delta^{15}N$ and concentration data, local measurements of the main trace gases (accept VOCs) and meteorology (temperature, relative humidity, wind) were available. In addition, detailed local primary
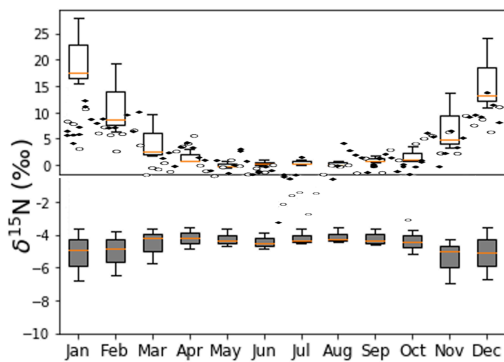
Figure 15. Upper panel is the observed NO_3^- $\delta^{15}N$ values of PM in the city of Tucson (Riha, 2013) and box and whisker plots values predicted by i_NRACM (1 week simulation, Red line = median, box = 1st and 3rd quantile, whisker is minimum and maximum). The bottom box and whisker plots are for i_NRACM simulations with R39 $^{15}\alpha$= 0.9971 from Freyer (1991).

24

pollutant emission inventories have been developed (Diem and Comrie, 2001). Tucson is a city with little industry or power generation so roughly 80% of the NO_x is due to vehicles and the relative proportion of all NOx sources is invariant throughout the year (Fig. S1). Further, Tucson is surrounded by a desert landscape and by and large not influences by regional pollution sources outside the city. i_NRACM was initialized with observed trace gas concentrations and NO_x and VOC emissions were based on previous work (Riha, 2013) and the source NO_x $\delta^{15}N$ value was set to -3‰, typical of vehicle emissions (Walter et al., 2015) and run for 1 week from the first day of each month. The aerosol surface area used to calculate k_{N2O5} was based on monthly average PM mass (Fig. S2) . The predicted NO_3^- (as HNO_3) $\delta^{15}N$ values (After 36 ± 12 hours) matched remarkably well with the observed $\delta^{15}N$ values in $PM_{2.5}$ and PM_{10} (Fig. 15). Observed maximums were in the winter months, peaking January at 15‰ close to the model maximum in January of 17%. The minimum $\delta^{15}N$ values (-2‰) are measured in July, similar to model predictions of 0‰ during July. The model captures the seasonal trend quite well, including the Spring plateau. This suggests that at this location, the observed seasonal variation in PM NO_3^- $\delta^{15}N$ values can be explained isotope effects associated with the photochemical conversion of NO_x into HNO_3. The wider range in HNO_3 $\delta^{15}N$ values in the winter months relative to summer months is due to difference in sunlight and oxidant loads. In winter sunlight hours are at a minimum (8.5 hours versus 12.8 in June) and ozone mixing ratios are a factor of 4-5 lower compared to the summer months (Riha, 2013). This results in rapid conversion of NO_x into HNO_3 in the summer the $HNO_3/(HNO_3+NO_x)$ exceeds 0.90 within two days whereas it requires six days during the winter (Fig. S3). The result is that in the summer HNO_3 $\delta^{15}N$ values rapidly approach the $\delta^{15}N$ of the NO_x source, whereas in the winter there is greater diurnal and daily variability until the very end of the simulation. The rapid swings in HNO_3 $\delta^{15}N$ values are thus a function of the chemical lifetime of NO_x and physical lifetime of HNO_3 with respect to wet (and dry) deposition. Thus, when the atmosphere is cleansed by regional rainfall, the isotope effects associated with photochemical oxidation will have a greater influence relative to NO_x sources and this is a plausible explanation of rapid changes in the $\delta^{15}N$ of rain nitrate over the course of a storm (*Rose et al., 2019*).

4. Conclusion

We have developed the first 0-D photochemical box model for ^{15}N compounds in the tropospheric NO_x-NO_y cycle. It was shown that of the 100's of N reactions in the RACM mechanism only a handful significantly impact the $\delta^{15}N$ of the main NO_y compounds (NO_x, HONO, HNO_3). Primarily these reactions are Leighton cycle reactions, $NO_2 + OH$, and NO_x isotope exchange, with N_2O_5 and nitrate radical reactions having a significant, but minor influence on NO_y $\delta^{15}N$ values. The model accuracy and its validation could be improved with additional research. The i_NRACM model could be refined by additional theoretical and/or experimental determination of the isotope fractionation factors for the N reactions. First and foremost, the fractionation factor for the $NO_2 + OH$ reaction needs evaluating in a more robust manner. Likewise, the fractionation factor for the $NO + OH$, another 3-body reaction, will have a large influence on HONO $\delta^{15}N$ values and determining its value will be key for interesting future HONO $\delta^{15}N$ data. The fractionation factor for NO_2 photolysis requires attention given the limitation of the ΔZPE PHIFE model [*Blake et al.*, *2003; Liang et al., 2004; Miller and Yung, 2000*]. On the validation end, the simultaneous measurement of $\delta^{15}N$ in multiple NO_y compounds would expose the accuracy or limitations of the i_NRACM model in a quantitative way. The i_NRACM model reproduced observed $\delta^{15}N$ data from year-long study on the isotopic composition of particulate nitrate collected in Tucson AZ. This

suggests that the model, which is publicly available, could be used as an analytical tool for researchers using 15N to gain insight into NO_x sources and transformation chemistry.

The i_NRACM model is the first step in our development of N isotope enabled 3-D chemical transport model (i_NCMAQ). That model will couple i_NRACM with a ^{15}NOx emissions model (i_NNEI) and WRF generated transport. The i_NRACM results show that photochemistry is an important control on the $\delta^{15}N$ of the NO_y compounds, in particular NO_3^-, for which there is a large and growing data set that can be used to validate the model. This is important because this suggests that $\delta^{15}N$ in NOy compounds could be used as a validation of different photochemical mechanisms. Further, if the photochemical effect can be deconvoluted from the observations then observed NO_y $\delta^{15}N$ could be used as a constraint and validation of NO_x emissions inventories. Expanded to the global scale, such a model could potentially be used to investigate the cause of $\delta^{15}N$ versions in NO_3^- found in Antarctic and Greenland ice cores (Hastings et al., 2009) and linked to historical changes in NO_x emission and NO_y chemistry.

Deleted: Repeating these simultaneous measurements in a range of environments would test the predictions made by out test case simulations.

Formatted: Subscript

Deleted: N isotopes in

Formatted: Superscript

Deleted: with

Formatted: Subscript

References

Aldener, M., Brown, S. S., Stark, H., Williams, E. J., Lerner, B. M., Kuster, W. C., ... & Ravishankara, A. R. (2006). Reactivity and loss mechanisms of NO_3 and N_2O_5 in a polluted marine environment: Results from in situ measurements during New England Air Quality Study 2002. *Journal of Geophysical Research: Atmospheres*, *111*(D23).

Altshuller, A. P. (1989). Nonmethane organic compound to nitrogen oxide ratios and organic composition in cities and rural areas. *JAPCA*, *39*(7), 936-943.

Andreae, M. O., and P. J. Crutzen (1997), Atmospheric aerosols: biogeochemical sources and role in atmospheric chemistry, *Science*, *276*(5315), 1052-1058.

Anttila, T., Kiendler-Scharr, A., Tillmann, R., & Mentel, T. F. (2006). On the reactive uptake of gaseous compounds by organic-coated aqueous aerosols: Theoretical analysis and application to the heterogeneous hydrolysis of N_2O_5. *The Journal of Physical Chemistry A*, *110*(35), 10435-10443.

Atkinson, R. (1990), Gas-phase tropospheric chemistry of organic-compounds - a review, *Atmospheric Environment Part a-General Topics*, *24*(1), 1-41, doi:10.1016/0960-1686(90)90438-s.

Atkinson, R. (2000), Atmospheric chemistry of VOCs and NO_x, *Atmospheric Environment*, *34*(12-14), 2063-2101.

Atkinson, R., D. L. Baulch, R. A. Cox, R. F. Hampson, J. A. Kerr, and J. Troe (1992), Evaluated kinetic and photochemical data for atmospheric chemistry supplement-iv - IUPAC subcommittee on gas kinetic data evaluation for atmospheric chemistry, *Journal of Physical and Chemical Reference Data*, *21*(6), 1125-1568, doi:10.1063/1.555918.

Bauer, S. E., D. Koch, N. Unger, S. M. Metzger, D. T. Shindell, and D. G. Streets (2007), Nitrate aerosols today and in 2030: a global simulation including aerosols and tropospheric ozone, *Atmospheric Chemistry and Physics*, *7*(19), 5043-5059

Baugues, K. (1986). *Review of NMOC, NOx and NMOC/NOx ratios measured in 1984 and 1985* (No. PB-87-166963/XAB; EPA-450/4-86/015). Environmental Protection Agency, Research Triangle Park, NC (USA). Monitoring and Data Analysis Div..

Bertram, T. H., & Thornton, J. A. (2009). Toward a general parameterization of N_2O_5 reactivity on aqueous particles: the competing effects of particle liquid water, nitrate and chloride. *Atmospheric Chemistry and Physics*, *9*(21), 8351-8363.

Bigeleisen, J. (1958), Second-Order Sum Rule for the Vibrations of Isotopic Molecules and the Second Rule of the Mean, *The Journal of Chemical Physics*, *28*(4), 694-699.

Bigeleisen, J., and M. G. Mayer (1947), Calculation of Equilibrium Constants for Isotopic Exchange Reactions, *The Journal of Chemical Physics*, *15*(5), 261-267.

Deleted:

27

Bigeleisen, J., and M. Wolfsberg (1958), Theoretical and experimental aspects of isotope effects in chemical kinetics, *Advances in Chem. Phys. (Prigogine, I. Interscience Publishers, Inc. , New York)*, *1*, 15-76.

Blake, G. A., M. C. Liang, C. G. Morgan, and Y. L. Yung (2003), A born-oppenheimer photolysis model of N_2O fractionation, *Geophysical Research Letters*, *30*(12), 58/51-58/54.

Bloss, W. J., M. J. Evans, J. D. Lee, R. Sommariva, D. E. Heard, and M. J. Pilling (2005), The oxidative capacity of the troposphere: Coupling of field measurements of OH and a global chemistry transport model, *Faraday Discussions*, *130*, 425-436.

Bottenheim, J. W., Gallant, A. G., & Brice, K. A. (1986). Measurements of NOy species and O3 at 82 N latitude. *Geophysical Research Letters*, *13*(2), 113-116.

Brimblecombe, P., H. Hara, and D. Houle (2007), *Acid Rain - Deposition to Recovery*, Springer.

Brown, S. S., J. B. Burkholder, R. K. Talukdar, and A. R. Ravishankara (2001), Reaction of hydroxyl radical with nitric acid: insights into its mechanism, *Journal of Physical Chemistry A*, *105*(9), 1605-1614.

Brown, L. L., & Begun, G. M. (1959). Nitrogen isotopic fractionation between nitric acid and the oxides of nitrogen. *The Journal of Chemical Physics*, *30*(5), 1206-1209.

Brown, S. S., et al. (2006), Variability in nocturnal nitrogen oxide processing and its role in regional air quality, *Science*, *311*(5757), 67-70.

Bruningfann, C. S., and J. B. Kaneene (1993), The Effects of Nitrate, Nitrite and N-Nitroso Compounds on Human Health - A Review, *Veterinary and Human Toxicology*, *35*(6), 521-538.

Carroll, M. A., Ridley, B. A., Montzka, D. D., Hubler, G., Walega, J. G., Norton, R. B., ... & Grahek, F. E. (1992). Measurements of nitric oxide and nitrogen dioxide during the Mauna Loa Observatory Photochemistry Experiment. *Journal of Geophysical Research: Atmospheres*, *97*(D10), 10361-10374.

Cao, Z. Y., X. H. Zhou, Y. J. Ma, L. P. Wang, R. D. Wu, B. Chen, and W. X. Wang (2017), The Concentrations, Formations, Relationships and Modeling of Sulfate, Nitrate and Ammonium (SNA) Aerosols over China, *Aerosol and Air Quality Research*, *17*(1), 84-97, doi:10.4209/aaqr.2016.01.0020.

Chai, J. J., and M. G. Hastings (2018), Collection Method for Isotopic Analysis of Gaseous Nitrous Acid, *Analytical Chemistry*, *90*(1), 830-838, doi:10.1021/acs.analchem.7b03561.

Chang, W. L., P. V. Bhave, S. S. Brown, N. Riemer, J. Stutz, and D. Dabdub (2011), Heterogeneous Atmospheric Chemistry, Ambient Measurements, and Model Calculations of N_2O_5: A Review, *Aerosol Science and Technology*, *45*(6), 665-695.

Charlson, R. J., S. E. Schwartz, J. M. Hales, R. D. Cess, J. A. Coakley, J. E. Hansen, and D. J. Hofmann (1992), Climate Forcing by Anthropogenic Aerosols, *Science*, *255*(5043), 423-430.

Chen, W. T., H. Liao, and J. H. Seinfeld (2007), Future climate impacts of direct radiative forcing of anthropogenic aerosols, tropospheric ozone, and long-lived greenhouse gases, *Journal of Geophysical Research-Atmospheres*, *112*(D14).

Cleveland, W. S., Kleiner, B., McRae, J. E., Warner, J. L., & Pasceri, R. E. (1977). Geographical properties of ozone concentrations in the northeastern United States. *Journal of the Air Pollution Control Association*, *27*(4), 325-328.

Cooper, O. R., Gao, R. S., Tarasick, D., Leblanc, T., & Sweeney, C. (2012). Long-term ozone trends at rural ozone monitoring sites across the United States, 1990–2010. *Journal of Geophysical Research: Atmospheres*, *117*(D22).

Davis, J. M., Bhave, P. V., & Foley, K. M. (2008). Parameterization of N_2O_5 reaction probabilities on the surface of particles containing ammonium, sulfate, and nitrate. *Atmospheric Chemistry and Physics*, *8*(17), 5295-5311.

Day, D. A., M. B. Dillon, P. J. Wooldridge, J. A. Thornton, R. S. Rosen, E. C. Wood, and R. C. Cohen (2003), On alkyl nitrates, O_3, and the "missing NO_y", *Journal of Geophysical Research-Atmospheres*, *108*(D16), doi:10.1029/2003jd003685.

DeMore, W. B., S. P. Sander, D. M. Golden, R. F. Hampson, M. J. Kurylo, C. J. Howard, A. R. Ravishankara, C. E. Kolb, and M. J. Molina, (1994), Chemical kinetics and photochemical data for use in stratospheric modeling, Eval. 11, *Natl. Aeronaut. and Space Admin., Jet Propul. Lab.*

Dentener, F. J., and P. J. Crutzen (1993), Reaction of nitrogen pentoxide on tropospheric aerosols: Impact on the global distributions of NO_x, ozone, and hydroxyl, *Journal of Geophysical Research*, *98*(D4), 7149-7163.

Diem, J. E., & Comrie, A. C. (2001). Allocating anthropogenic pollutant emissions over space: application to ozone pollution management. *Journal of environmental management*, *63*(4), 425-447.

Du, E. Z., M. E. Fenn, W. De Vries, and Y. S. Ok (2019), Atmospheric nitrogen deposition to global forests: Status, impacts and management options, *Environmental Pollution*, *250*, 1044-1048, doi:10.1016/j.envpol.2019.04.014.

Elliott, E. M., C. Kendall, E. W. Boyer, D. A. Burns, G. G. Lear, H. E. Golden, K. Harlin, A. Bytnerowicz, T. J. Butler, and R. Glatz (2009), Dual nitrate isotopes in dry deposition: Utility for partitioning NO_x source contributions to landscape nitrogen deposition, *Journal of Geophysical Research-Biogeosciences*, *114*.

Elliott, E. M., C. Kendall, S. D. Wankel, D. A. Burns, E. W. Boyer, K. Harlin, D. J. Bain, and T. J. Butler (2007), Nitrogen isotopes as indicators of NOx source contributions to atmospheric nitrate

deposition across the Midwestern and northeastern United States, *Environmental Science & Technology*, *41*(22), 7661-7667.

Elliott, E. M., Z. J. Yu, A. S. Cole, and J. G. Coughlin (2019), Isotopic advances in understanding reactive nitrogen deposition and atmospheric processing, *Science of the Total Environment*, *662*, 393-403, doi:10.1016/j.scitotenv.2018.12.177.

Fahey, D. W., Hübler, G., Parrish, D. D., Williams, E. J., Norton, R. B., Ridley, B. A., ... & Fehsenfeld, F. C. (1986). Reactive nitrogen species in the troposphere: Measurements of NO, NO_2, HNO_3, particulate nitrate, peroxyacetyl nitrate (PAN), O_3, and total reactive odd nitrogen (NO_y) at Niwot Ridge, Colorado. *Journal of Geophysical Research: Atmospheres*, *91*(D9), 9781-9793.

Felix, J. D., and E. M. Elliott (2014), Isotopic composition of passively collected nitrogen dioxide emissions: Vehicle, soil and livestock source signatures, *Atmospheric Environment*, *92*, 359-366, doi:10.1016/j.atmosenv.2014.04.005.

Felix, J. D., E. M. Elliott, and S. L. Shaw (2012), Nitrogen Isotopic Composition of Coal-Fired Power Plant NO_x: Influence of Emission Controls and Implications for Global Emission Inventories, *Environmental Science & Technology*, *46*(6), 3528-3535.

Felix, J. D., Elliott, E. M., Avery, G. B., Kieber, R. J., Mead, R. N., Willey, J. D., & Mullaugh, K. M. (2015). Isotopic composition of nitrate in sequential Hurricane Irene precipitation samples: implications for changing NO_x sources. *Atmospheric Environment*, *106*, 191-195.

Fibiger, D. L., and M. G. Hastings (2016), First Measurements of the Nitrogen Isotopic Composition of NO_x from Biomass Burning, *Environmental Science & Technology*, *50*(21), 11569-11574, doi:10.1021/acs.est.6b03510.

Finlayson-Pitts, B. J., and J. N. Pitts, Jr. (2000), *Chemistry of the Upper and Lower Atmosphere*, Academic Press, San Diego.

Fowler, D., et al. (2013), The global nitrogen cycle in the twenty-first century, *Philosophical Transactions of the Royal Society B-Biological Sciences*, *368*(1621).

Freyer, H. D. (1991). Seasonal-Variation of $^{15}N/^{14}N$ Ratios in Atmospheric Nitrate Species. *Tellus Series B-Chemical and Physical Meteorology*, *43*(1), 30-44.

Freyer, H. D., D. Kley, A. Volzthomas, and K. Kobel (1993), On the interaction of isotopic exchange processes with photochemical-reactions in atmospheric oxides of nitrogen, *Journal of Geophysical Research-Atmospheres*, *98*(D8), 14791-14796, doi:10.1029/93jd00874.

Fuentes, J. D., Chamecki, M., Nascimento dos Santos, R. M., Von Randow, C., Stoy, P. C., Katul, G., ... & Souza Freire, L. (2016). Linking meteorology, turbulence, and air chemistry in the Amazon rain forest. *Bulletin of the American Meteorological Society*, *97*(12), 2329-2342.

Galloway, J. N., Dentener, F. J., Capone, D. G., Boyer, E. W., Howarth, R. W., Seitzinger, S. P., . & Karl, D. M. (2004). Nitrogen cycles: past, present, and future. *Biogeochemistry*, *70*(2), 153-226.

Golden, D. M., and G. P. Smith (2000), Reaction of OH + NO_2 + M: A new view, *Journal of Physical Chemistry A*, *104*(17), 3991-3997.

Greenberg, J. P., & Zimmerman, P. R. (1984). Nonmethane hydrocarbons in remote tropical, continental, and marine atmospheres. *Journal of Geophysical Research: Atmospheres*, *89*(D3), 4767-4778.

Gregory, G. L., Browell, E. V., & Warren, L. S. (1988). Boundary layer ozone: An airborne survey above the Amazon Basin. *Journal of Geophysical Research: Atmospheres*, *93*(D2), 1452-1468.

Hall, J. V., A. M. Winer, M. T. Klienman, F. W. Lurmann, V. Brajer, and S. D. Colome (1992), Valuing the Health Benefits of Clean Air, *Science*, *V255*, 812-817.

Hagenbjörk, A., Malmqvist, E., Mattisson, K., Sommar, N. J., & Modig, L. (2017). The spatial variation of O_3, NO, NO_2 and NO_x and the relation between them in two Swedish cities. *Environmental monitoring and assessment*, *189*(4), 161.

Harrison, R. M., J. L. Grenfell, S. Yamulki, K. C. Clemitshaw, S. A. Penkett, J. N. Cape, and G. G. McFadyen (1999), Budget of NO_y species measured at a coastal site, *Atmospheric Environment*, *33*(26), 4255-4272, doi:10.1016/s1352-2310(99)00176-4.

Hastings, M. G., K. L. Casciotti, and E. M. Elliott (2013), Stable Isotopes as Tracers of Anthropogenic Nitrogen Sources, Deposition, and Impacts, *Elements*, *9*(5), 339-344.

Hastings, M. G., Sigman, D. M., & Lipschultz, F. (2003). Isotopic evidence for source changes of nitrate in rain at Bermuda. *Journal of Geophysical Research: Atmospheres*, *108*(D24).

He, H., Stehr, J. W., Hains, J. C., Krask, D. J., Doddridge, B. G., Vinnikov, K. Y., ... & Dickerson, R. R. (2013). Trends in emissions and concentrations of air pollutants in the lower troposphere in the Baltimore/Washington airshed from 1997 to 2011. *Atmospheric Chemistry and Physics*, *13*(15), 7859-7874.

Heaton, T. H. E. (1987). 15N 14N ratios of nitrate and ammonium in rain at Pretoria, South Africa. *Atmospheric Environment (1967)*, *21*(4), 843-852.

Hegglin, M. I., D. Brunner, T. Peter, P. Hoor, H. Fischer, J. Staehelin, M. Krebsbach, C. Schiller, U. Parchatka, and U. Weers (2006), Measurements of NO, NO_y, N_2O, and O_3 during SPURT: implications for transport and chemistry in the lowermost stratosphere, *Atmospheric Chemistry and Physics*, *6*, 1331-1350, doi:10.5194/acp-6-1331-2006.

Horowitz, L. W., J. Liang, G. M. Gardner, and D. J. Jacob (1998), Export of reactive nitrogen from North America during summertime: sensitivity to hydrocarbon chemistry, *Journal of Geophysical Research*, *103*(D11), 13451-13476.

Houlton, B. Z., Boyer, E., Finzi, A., Galloway, J., Leach, A., Liptzin, D., ... & Townsend, A. R. (2013). Intentional versus unintentional nitrogen use in the United States: trends, efficiency and implications. *Biogeochemistry*, *114*(1-3), 11-23.

Hoyle, C. R., et al. (2011), A review of the anthropogenic influence on biogenic secondary organic aerosol, *Atmospheric Chemistry and Physics*, *11*(1), 321-343, doi:10.5194/acp-11-321-2011.

Hudman, R. C., Moore, N. E., Mebust, A. K., Martin, R. V., Russell, A. R., Valin, L. C., & Cohen, R. C. (2012). Steps towards a mechanistic model of global soil nitric oxide emissions: implementation and space based-constraints. *Atmospheric Chemistry and Physics*, *12*(16), 7779-7795.

Jaffe, D. A., Honrath, R. E., Zhang, L., Akimoto, H., Shimizu, A., Mukai, H., ... & Merrill, J. (1996). Measurements of NO, NO_y, CO and O_3 and estimation of the ozone production rate at Oki Island, Japan, during PEM-West. *Journal of Geophysical Research: Atmospheres*, *101*(D1), 2037-2048.

Janach, W. E. (1989). Surface ozone: trend details, seasonal variations, and interpretation. *Journal of Geophysical Research: Atmospheres*, *94*(D15), 18289-18295.
Kirchhoff, V. W. (1988). Surface ozone measurements in Amazonia. *Journal of Geophysical Research: Atmospheres*, *93*(D2), 1469-1476.

Kastler, J., & Ballschmiter, K. (1998). Bifunctional alkyl nitrates–trace constituents of the atmosphere. *Fresenius' journal of analytical chemistry*, *360*(7-8), 812-816.

Kuang, C., Riipinen, I., Sihto, S. L., Kulmala, M., McCormick, A. V., & McMurry, P. H. (2010). An improved criterion for new particle formation in diverse atmospheric environments. *Atmospheric Chemistry and Physics*, *10*(17), 8469-8480.

Lajtha, K., and J. Jones (2013), Trends in cation, nitrogen, sulfate and hydrogen ion concentrations in precipitation in the United States and Europe from 1978 to 2010: a new look at an old problem, *Biogeochemistry*, *116*(1-3), 303-334, doi:10.1007/s10533-013-9860-2.
Lelieveld, J., et al. (2008), Atmospheric oxidation capacity sustained by a tropical forest, *Nature*, *452*(7188), 737-740.

Lee, S. H., Uin, J., Guenther, A. B., de Gouw, J. A., Yu, F., Nadykto, A. B., ... & Baumann, K. (2016). Isoprene suppression of new particle formation: Potential mechanisms and implications. *Journal of Geophysical Research: Atmospheres*, *121*(24), 14-621.

Lefohn, A. S., & Pinkerton, J. E. (1988). High resolution characterization of ozone data for sites located in forested areas of the United States. *JAPCA*, *38*(12), 1504-1511.

Liang, M. C., G. A. Blake, and Y. L. Yung (2004), A semianalytic model for photo-induced isotopic fractionation in simple molecules, *Journal of Geophysical Research-Atmospheres*, *109*(D10).

Logan, J. A. (1989). Ozone in rural areas of the United States. *Journal of Geophysical Research: Atmospheres*, *94*(D6), 8511-8532.

Ma, J. Z., Y. C. Liu, C. Han, Q. X. Ma, C. Liu, and H. He (2013), Review of heterogeneous photochemical reactions of NOy on aerosol - A possible daytime source of nitrous acid (HONO) in the atmosphere, *Journal of Environmental Sciences-China*, *25*(2), 326-334, doi:10.1016/s1001-0742(12)60093-x.

Ma, Z., Liu, C., Zhang, C., Liu, P., Ye, C., Xue, C., ... & Mu, Y. (2019). The levels, sources and reactivity of volatile organic compounds in a typical urban area of Northeast China. *Journal of Environmental Sciences*, *79*, 121-134.

Madronich, S. (1987). Photodissociation in the atmosphere: 1. Actinic flux and the effects of ground reflections and clouds. *Journal of Geophysical Research: Atmospheres*, *92*(D8), 9740-9752.

McMurry, P. H., Fink, M., Sakurai, H., Stolzenburg, M. R., Mauldin III, R. L., Smith, J., ... & Huey, L. G. (2005). A criterion for new particle formation in the sulfur-rich Atlanta atmosphere. *Journal of Geophysical Research: Atmospheres*, *110*(D22).

Michalski, G., R. Jost, D. Sugny, M. Joyeux, and M. Thiemens (2004), Dissociation energies of six NO_2 isotopologues by laser induced fluorescence and zero point energy of some triatomic molecules *Journal of Chemical Physics*, *121*(15), 7153-7161.

Miller, C. E., and Y. L. Yung (2000), Photo-induced isotopic fractionation, *Journal of Geophysical Research-Atmospheres*, *105*(D23), 29039-29051.

Morino, Y., Y. Kondo, N. Takegawa, Y. Miyazaki, K. Kita, Y. Komazaki, M. Fukuda, T. Miyakawa, N. Moteki, and D. R. Worsnop (2006), Partitioning of HNO_3 and particulate nitrate over Tokyo: Effect of vertical mixing, *Journal of Geophysical Research-Atmospheres*, *111*(D15), doi:10.1029/2005jd006887.

Moore, H. (1977). The isotopic composition of ammonia, nitrogen dioxide and nitrate in the atmosphere. *Atmospheric Environment (1967)*, *11*(12), 1239-1243.

National Research Council. (1992). *Rethinking the ozone problem in urban and regional air pollution*. National Academies Press.

Pan, Y. P., S. L. Tian, D. W. Liu, Y. T. Fang, X. Y. Zhu, M. Gao, G. R. Wentworth, G. Michalski, X. J. Huang, and Y. S. Wang (2018), Source Apportionment of Aerosol Ammonium in an Ammonia-Rich Atmosphere: An Isotopic Study of Summer Clean and Hazy Days in Urban Beijing, *Journal of Geophysical Research-Atmospheres*, *123*(10), 5681-5689, doi:10.1029/2017jd028095.

33

Parrish, D. D., Trainer, M., Williams, E. J., Fahey, D. W., Hübler, G., Eubank, C. S., ... & Fehsenfeld, F. C. (1986). Measurements of the NO_x-O_3 photostationary state at Niwot Ridge, Colorado. *Journal of Geophysical Research: Atmospheres*, *91*(D5), 5361-5370.

Paulot, F., P. Ginoux, W. F. Cooke, L. J. Donner, S. Fan, M. Y. Lin, J. Mao, V. Naik, and L. W. Horowitz (2016), Sensitivity of nitrate aerosols to ammonia emissions and to nitrate chemistry: implications for present and future nitrate optical depth, *Atmospheric Chemistry and Physics*, *16*(3), 1459-1477, doi:10.5194/acp-16-1459-2016.

Petäjä, T., Mauldin Iii, R. L., Kosciuch, E., McGrath, J., Nieminen, T., Paasonen, P., ... & Kulmala, M. (2009). Sulfuric acid and OH concentrations in a boreal forest site. *Atmospheric Chemistry and Physics*, *9*(19), 7435-7448.

Pilegaard, K. (2013). Processes regulating nitric oxide emissions from soils. *Phil. Trans. R. Soc. B*, *368*(1621), 20130126

Platt, U. F., A. M. Winer, H. W. Biermann, R. Atkinson, and J. N. Pitts (1984), Measurement of Nitrate Radical Concentrations in Continental Air, *Environmental Science & Technology*, *18*(5), 365-369.

Prinn, R. G. (2003), The cleansing capacity of the atmosphere, *Annual Review of Environment and Resources*, *28*, 29-57.

Pusede, S. E., et al. (2016), On the effectiveness of nitrogen oxide reductions as a control over ammonium nitrate aerosol, *Atmospheric Chemistry and Physics*, *16*(4), 2575-2596, doi:10.5194/acp-16-2575-2016.

Pye, H. O. T., A. W. H. Chan, M. P. Barkley, and J. H. Seinfeld (2010), Global modeling of organic aerosol: the importance of reactive nitrogen (NO_x and NO_3), *Atmospheric Chemistry and Physics*, *10*(22), 11261-11276.

Qi, X. M., Ding, A. J., Nie, W., Petäjä, T., Kerminen, V. M., Herrmann, E., and Sun, J. N. (2015). Aerosol size distribution and new particle formation in the western Yangtze River Delta of China: 2 years of measurements at the SORPES station. *Atmospheric chemistry and physics*, *15*(21), 12445-12464.

Richet, P., Y. Bottinga, and M. Javoy (1977), Review of hydrogen, carbon, nitrogen, oxygen, sulfur, and chlorine stable isotope fractionation among gaseous molecules, *Annual Review of Earth and Planetary Sciences*, *5*, 65-110

Riemer, N., Vogel, H., Vogel, B., Anttila, T., Kiendler-Scharr, A., and Mentel, T. F. (2009). Relative importance of organic coatings for the heterogeneous hydrolysis of N_2O_5 during summer in Europe. *Journal of Geophysical Research: Atmospheres*, *114*(D17).

Riemer, N., H. Vogel, B. Vogel, B. Schell, I. Ackermann, C. Kessler, and H. Hass (2003), Impact of the heterogeneous hydrolysis of N_2O_5 on chemistry and nitrate aerosol formation in the lower

troposphere under photosmog conditions, *Journal of Geophysical Research*, *108*(D4), 4144-DOI: 4110.1029/2002JD002436.

Riha, K. M. (2013). The use of stable isotopes to constrain the nitrogen cycle. Purdue University, West Lafayette, IN.

Roehl, C. M., J. J. Orlando, G. S. Tyndall, R. E. Shetter, G. J. Vazquez, C. A. Cantrell, and J. G. Calvert (1994), Temperature-dependence of the quantum yields for the photolysis of NO_2 near the dissociation limit, *Journal of Physical Chemistry*, *98*(32), 7837-7843, doi:10.1021/j100083a015.

Romer, P. S., Duffey, K. C., Wooldridge, P. J., Allen, H. M., Ayres, B. R., Brown, S. S., ... & Feiner, P. A. (2016). The lifetime of nitrogen oxides in an isoprene-dominated forest. *Atmospheric Chemistry and Physics*, *16*(12), 7623-7637.

Rose, L. A., Yu, Z. J., Bain, D. J., & Elliott, E. M. (2019). High resolution, extreme isotopic variability of precipitation nitrate. *Atmospheric Environment, 207*, 63-74. 10.1016/j.atmosenv.2019.03.012

Saito, T., Yokouchi, Y., & Kawamura, K. (2000). Distributions of C^2–C^6 hydrocarbons over the western North Pacific and eastern Indian Ocean. *Atmospheric environment*, *34*(25), 4373-4381.

Savard, M. M., Cole, A., Smirnoff, A., & Vet, R. (2017). δ15N values of atmospheric N species simultaneously collected using sector-based samplers distant from sources–Isotopic inheritance and fractionation. *Atmospheric environment*, *162*, 11-22.

Sharma, H. D., R. E. Jervis, and K. Y. Wong (1970), Isotopic exchange reactions in nitrogen oxides, *Journal of Physical Chemistry*, *74*(4), 923-933.

Shepherd, M. F., Barzetti, S., & Hastie, D. R. (1991). The Production of Atmospheric NO_2 and N_2O from a Fertilized Agricultural Soil.

Shrivastava, M., Cappa, C. D., Fan, J., Goldstein, A. H., Guenther, A. B., Jimenez, J. L., ... & Petaja, T. (2017). Recent advances in understanding secondary organic aerosol: Implications for global climate forcing. *Reviews of Geophysics*, *55*(2), 509-559.

Sjostedt, S. J., Slowik, J. G., Brook, J. R., Chang, R. W., Mihele, C., Stroud, C. A., ... & Abbatt, J. P. D. (2011). Diurnally resolved particulate and VOC measurements at a rural site: indication of significant biogenic secondary organic aerosol formation. *Atmospheric Chemistry and Physics*, *11*(12), 5745-5760.

Snyder, J. A., D. Hanway, J. Mendez, A. J. Jamka, and F. M. Tao (1999), A density functional theory study of the gas-phase hydrolysis of dinitrogen pentoxide, *Journal of Physical Chemistry A*, *103*(46), 9355-9358.

Spak, S. N., and T. Holloway (2009), Seasonality of speciated aerosol transport over the Great Lakes region, *Journal of Geophysical Research-Atmospheres*, *114*.

Srivastava, R. K., Neuffer, W., Grano, D., Khan, S., Staudt, J. E., & Jozewicz, W. (2005). Controlling NO_x emission from industrial sources. *Environmental progress*, *24*(2), 181-197.

Seinfeld, J. H., and S. N. Pandis (1998), *Atmospheric chemistry and physics : from air pollution to climate change*, 1 ed., New York : Wiley.

Stockwell, W. R., F. Kirchner, M. Kuhn, and S. Seefeld (1997), A new mechanism for regional atmospheric chemistry modeling, *Journal of Geophysical Research*, *102*(D22), 25847-25879.

Stockwell, W. R., P. Middleton, J. S. Chang, and X. Y. Tang (1990), The 2nd Generation Regional Acid Deposition Model Chemical Mechanism for Regional Air-Quality Modeling, *Journal of Geophysical Research-Atmospheres*, *95*(D10), 16343-16367.

Torres, A. L., & Buchan, H. (1988). Tropospheric nitric oxide measurements over the Amazon Basin. *Journal of Geophysical Research: Atmospheres*, *93*(D2), 1396-1406.

Urey, H. C. (1947), Thermodynamic properties of isotopic substances, *J. Chem. Soc*, 562-581.

Van Hook, W. A., L. P. N. Rebelo, and M. Wolfsberg (2001), An interpretation of the vapor phase second virial coefficient isotope effect: Correlation of virial coefficient and vapor pressure isotope effects, *Journal of Physical Chemistry A*, *105*(40), 9284-9297, doi:10.1021/jp004305z.

Vandaele, A. C., C. Hermans, S. Fally, M. Carleer, R. Colin, M. F. Merienne, A. Jenouvrier, and B. Coquart (2002), High-resolution Fourier transform measurement of the NO_2 visible and near-infrared absorption cross sections: Temperature and pressure effects, *Journal of Geophysical Research-Atmospheres*, *107*(D18), doi:10.1029/2001jd000971.

Walters, W., S. Goodwin, Michalski, and G. (2015a), Nitrogen Stable Isotope Composition of Vehile Emitted NO_x, *Environemental Science and Technology*, *49*(4), 2278-2285.

Walters, W. W., H. Fang, and G. Michalski (2018), Summertime diurnal variations in the isotopic composition of atmospheric nitrogen dioxide at a small midwestern United States city, *Atmospheric Environment*, *179*, 1-11, doi:10.1016/j.atmosenv.2018.01.047.

Walters, W. W., and G. Michalski (2015), Theoretical calculation of nitrogen isotope equilibrium exchange fractionation factors for various NO_y molecules, *Geochimica Et Cosmochimica Acta*, *164*, 284-297, doi:10.1016/j.gca.2015.05.029.

Walters, W. W., and G. Michalski (2016), Ab initio study of nitrogen and position-specific oxygen kinetic isotope effects in the $NO + O_3$ reaction, *Journal of Chemical Physics*, *145*(22), doi:10.1063/1.4968562.

Walters, W. W., D. S. Simonini, and G. Michalski (2016), Nitrogen isotope exchange between NO and NO_2 and its implications for ^{15}N variations in tropospheric NO_x and atmospheric nitrate, *Geophysical Research Letters*, *43*(1), 440-448, doi:10.1002/2015gl066438.

Walters, W. W., B. D. Tharp, H. Fang, B. J. Kozak, and G. Michalski (2015b), Nitrogen Isotope Composition of Thermally Produced NOx from Various Fossil-Fuel Combustion Sources, *Environmental Science & Technology*, *49*(19), 11363-11371, doi:10.1021/acs.est.5b02769.

Wang, T., Xue, L., Brimblecombe, P., Lam, Y. F., Li, L., & Zhang, L. (2017). Ozone pollution in China: A review of concentrations, meteorological influences, chemical precursors, and effects. *Science of the Total Environment*, *575*, 1582-1596.

Williams, E. J., Parrish, D. D., & Fehsenfeld, F. C. (1987). Determination of nitrogen oxide emissions from soils: Results from a grassland site in Colorado, United States. *Journal of Geophysical Research: Atmospheres*, *92*(D2), 2173-2179.

Wolfsberg, M. (1960), Note on secondary isotope effects in reaction rates, *Journal of Chemical Physics*, *33*(1), 2-6, doi:10.1063/1.1731078.

Wolfsberg, M., W. A. Van Hook, P. Paneth, L. P. N. Rebelo, M. Wolfsberg, W. A. VanHook, and P. Paneth (2010), *Isotope Effects on Equilibrium Constants of Chemical Reactions; Transition State Theory of Isotope Effects*, 77-137 pp., doi:10.1007/978-90-481-2265-3_4.

Yang, J., Honrath, R. E., Peterson, M. C., Parrish, D. D., & Warshawsky, M. (2004). Photostationary state deviation–estimated peroxy radicals and their implications for HO_x and ozone photochemistry at a remote northern Atlantic coastal site. *Journal of Geophysical Research: Atmospheres*, *109*(D2).

Yu, Z., & Elliott, E. M. (2017). Novel method for nitrogen isotopic analysis of soil-emitted nitric oxide. *Environmental Science & Technology*, *51*(11), 6268-6278.

Zhang, Y., K. Vijayaraghavan, X. Y. Wen, H. E. Snell, and M. Z. Jacobson (2009), Probing into regional ozone and particulate matter pollution in the United States: 1. A 1 year CMAQ simulation and evaluation using surface and satellite data, *Journal of Geophysical Research-Atmospheres*, *114*.

Zimmerman, P. R., Greenberg, J. P., & Westberg, C. E. (1988). Measurements of atmospheric hydrocarbons and biogenic emission fluxes in the Amazon boundary layer. *Journal of Geophysical Research: Atmospheres*, *93*(D2), 1407-1416.